

# Radioactive contamination of scintillators

F.A. Danevich<sup>a,b</sup>, V.I. Tretyak<sup>a</sup>

<sup>a</sup>*Institute for Nuclear Research, Kyiv 03028, Ukraine*

<sup>b</sup>*CSNSM, Univ. Paris-Sud, CNRS/IN2P3, Univ. Paris-Saclay, 91405 Orsay, France*

## Abstract

Low counting experiments (search for double  $\beta$  decay and dark matter particles, measurements of neutrino fluxes from different sources, search for hypothetical nuclear and subnuclear processes, low background  $\alpha$ ,  $\beta$ ,  $\gamma$  spectrometry) require extremely low background of a detector. Scintillators are widely used to search for rare events both as conventional scintillation detectors and as cryogenic scintillating bolometers. Radioactive contamination of a scintillation material plays a key role to reach low level of background. Origin and nature of radioactive contamination of scintillators, experimental methods and results are reviewed. A programme to develop radiopure crystal scintillators for low counting experiments is discussed briefly.

Keywords: Scintillation detector; Rare decays; Low counting experiment; Radioactive contamination

PACS numbers: 29.40.Mc; 23.40.-s; 23.60.+e; 95.35.+d

## 1 Introduction

Search for neutrinoless double beta decay, dark matter particles, measurements of solar and reactor neutrino fluxes, tests of fundamental laws with increasing accuracy (e.g. Pauli exclusion principle, charge conservation, stability of nucleons, etc.), search for hypothetical particles and effects beyond the Standard Model (axions; charge, magnetic momentum, mass of neutrino; etc.) are the topics of astroparticle physics. Scintillation detectors possess a range of important properties for low counting experiments: presence of certain chemical elements (important in searches for double decay, investigations of rare  $\beta$  and  $\alpha$  decays) or variety of elements (which can be exploited in dark matter detectors to probe new areas of parameter space), large sensitive volume, reasonable energy resolution (very high in a case of cryogenic scintillating bolometers), low energy threshold, long time stability of operation, pulse-shape discrimination ability, low cost.

Radiopurity is a crucial property of scintillation material to reach low background counting rate of a detector. We review here application of scintillation materials in astroparticle physics, experimental methods to measure activities of radionuclides inside scintillators, origin and nature of radioactive contamination, radiopurity data for different scintillation materials. A programme to develop radiopure crystal scintillators for low counting experiments is discussed briefly. We do not consider here noble gas based low background scintillation detectors referring readers to the reviews [1, 2, 3].

## 2 Scintillators in astroparticle physics

### 2.1 Double $\beta$ decay

Observations of neutrino oscillations give clear evidence that neutrino is a massive particle (see e.g. [4, 5, 6, 7]). The neutrinoless double beta ( $0\nu 2\beta$ ) decay violates the lepton number conservation and is possible if neutrino is a Majorana particle (identical to its antiparticle) with non-zero mass [8]. The process is one of the ways to investigate properties of neutrino and weak interaction, and to test the Standard Model of particle physics [9, 10, 11, 12, 13, 14]. In particular, investigation of this phenomenon could allow to determine the absolute scale of the neutrino mass and the neutrino mass hierarchy. The  $0\nu 2\beta$  decay is still not observed despite the seventy years of searches (for the status of  $0\nu 2\beta$  decay searches we refer reader to the reviews [15, 16, 17, 18, 19, 20] and recent experiments [22, 24, 23, 21, 25]).

High sensitivity experiments to search for double  $\beta$  processes in different nuclei are strongly required both for theoretical and experimental reasons. Despite valuable theoretical efforts, there is a substantial difference in the  $0\nu 2\beta$  nuclear matrix elements (NME) calculated by using different nuclear models [26]. Therefore, the theory does not provide suggestions of a nucleus with the highest decay probability. From the experimental point of view, since  $0\nu 2\beta$  decay is expected to be an extremely rare process, detection of the decay in one nucleus naturally will call for support of the observation with other nuclei. Furthermore, development of experimental methods for different nuclei is required taking into account possible breakthroughs in experimental techniques [27]. The recent progress in low-temperature scintillating bolometers is a good example.

There are quite a big number of scintillation materials which contain double  $\beta$  active isotopes. For this reason scintillators are widely used in double  $\beta$  decay experiments. It is worth to mention a pioneer work of der Mateosian and Goldhaber to search for neutrinoless double  $\beta$  decay of  $^{48}\text{Ca}$  by using enriched and depleted in  $^{48}\text{Ca}$  calcium fluoride [ $\text{CaF}_2(\text{Eu})$ ] crystal scintillators [28]. During the last two decades several high sensitivity studies of the double  $\beta$  decay processes were performed using crystal scintillators with specific candidate nuclei. The most sensitive  $2\beta$  experiments with crystal scintillators are reported in Table 1.

Table 1: The most sensitive calorimetric  $2\beta$  experiments with scintillators. Half-life limits are given at 90% confidence level.

$2\beta$ transition	Scintillator	Main results: half-life (channels)	Reference
$^{40}\text{Ca} \rightarrow ^{40}\text{Ar}$	$\text{CaWO}_4$	$\geq 9.9 \times 10^{21}$ yr ( $2\nu 2K$ )	[29]
	$\text{CaWO}_4$	$\geq 1.4 \times 10^{22}$ yr ( $0\nu 2\varepsilon$ )	[29]
$^{46}\text{Ca} \rightarrow ^{46}\text{Ti}$	$\text{CaF}_2(\text{Eu})$	$\geq 1.0 \times 10^{17}$ yr ( $0\nu 2\beta^-$ )	[30]
$^{48}\text{Ca} \rightarrow ^{48}\text{Ti}$	$\text{CaF}_2(\text{Eu})$	$\geq 5.8 \times 10^{22}$ yr ( $0\nu 2\beta^-$ )	[31]
$^{70}\text{Zn} \rightarrow ^{70}\text{Ge}$	$\text{ZnWO}_4$	$\geq 3.8 \times 10^{18}$ yr ( $2\nu 2\beta^-$ )	[32]
	$\text{ZnWO}_4$	$\geq 3.2 \times 10^{19}$ yr ( $0\nu 2\beta^-$ )	[32]
$^{64}\text{Zn} \rightarrow ^{64}\text{Ni}$	$\text{ZnWO}_4$	$\geq 1.1 \times 10^{19}$ yr ( $2\nu 2K$ )	[32]
	$\text{ZnWO}_4$	$\geq 9.4 \times 10^{20}$ yr ( $2\nu\varepsilon\beta^+$ )	[32]
$^{82}\text{Se} \rightarrow ^{82}\text{Kr}$	$\text{Zn}^{82}\text{Se}$	$\geq 2.4 \times 10^{24}$ yr ( $0\nu 2\beta^-$ )	[33]
$^{100}\text{Mo} \rightarrow ^{100}\text{Ru}$	$\text{ZnMoO}_4$	$= [7.15 \pm 0.37(\text{stat.}) \pm 0.66(\text{syst.})] \times 10^{18}$ yr ( $2\nu 2\beta^-$ )	[34]
	$\text{Li}_2^{100}\text{MoO}_4$	$= [6.90 \pm 0.15(\text{stat.}) \pm 0.37(\text{syst.})] \times 10^{18}$ yr ( $2\nu 2\beta^-$ )	[35]
	$\text{Li}_2^{100}\text{MoO}_4$	$\geq 7.0 \times 10^{22}$ yr ( $0\nu 2\beta^-$ )	[36]
	$^{48}\text{depl}\text{Ca}^{100}\text{MoO}_4$	$\geq 4.0 \times 10^{21}$ yr ( $0\nu 2\beta^-$ )	[37]
$^{106}\text{Cd} \rightarrow ^{106}\text{Pd}$	$^{106}\text{CdWO}_4$	$\geq 1.1 \times 10^{21}$ yr ( $2\nu\varepsilon\beta^+$ )	[38]
	$^{106}\text{CdWO}_4$	$\geq 2.2 \times 10^{21}$ yr ( $0\nu\varepsilon\beta^+$ )	[39]
$^{108}\text{Cd} \rightarrow ^{108}\text{Pd}$	$\text{CdWO}_4$	$\geq 1.1 \times 10^{18}$ yr ( $2\nu 2K$ )	[40]
	$\text{CdWO}_4$	$\geq 1.0 \times 10^{18}$ yr ( $0\nu 2\varepsilon$ )	[40]
$^{114}\text{Cd} \rightarrow ^{114}\text{Sn}$	$\text{CdWO}_4$	$\geq 1.3 \times 10^{18}$ yr ( $2\nu 2\beta^-$ )	[40]
	$\text{CdWO}_4$	$\geq 1.1 \times 10^{21}$ yr ( $0\nu 2\beta^-$ )	[40]
$^{116}\text{Cd} \rightarrow ^{116}\text{Sn}$	$^{116}\text{CdWO}_4$	$= [2.69 \pm 0.02(\text{stat.}) \pm 0.14(\text{syst.})] \times 10^{19}$ yr ( $2\nu 2\beta^-$ )	[41]
	$^{116}\text{CdWO}_4$	$\geq 2.4 \times 10^{23}$ yr ( $0\nu 2\beta^-$ )	[41]
$^{136}\text{Xe} \rightarrow ^{136}\text{Ba}$	Xenon-loaded	$= [2.21 \pm 0.02(\text{stat.}) \pm 0.07(\text{syst.})] \times 10^{21}$ yr ( $2\nu 2\beta^-$ )	[25]
	liquid scintillator	$\geq 1.07 \times 10^{26}$ yr ( $0\nu 2\beta^-$ )	[25]
$^{130}\text{Ba} \rightarrow ^{130}\text{Xe}$	$\text{BaF}_2$	$\geq 1.4 \times 10^{17}$ yr ( $0\nu\varepsilon\beta^+$ )	[42]
$^{136}\text{Ce} \rightarrow ^{136}\text{Ba}$	$\text{CeCl}_3$	$\geq 3.2 \times 10^{16}$ yr ( $2\nu 2K$ )	[43]
$^{160}\text{Gd} \rightarrow ^{160}\text{Dy}$	$\text{Gd}_2\text{SiO}_5(\text{Ce})$	$\geq 1.9 \times 10^{19}$ yr ( $2\nu 2\beta^-$ )	[44]
	$\text{Gd}_2\text{SiO}_5(\text{Ce})$	$\geq 1.3 \times 10^{21}$ yr ( $0\nu 2\beta^-$ )	[44]
$^{180}\text{W} \rightarrow ^{180}\text{Hf}$	$\text{CaWO}_4$	$\geq 3.1 \times 10^{19}$ yr ( $2\nu 2K$ )	[29]
	$\text{CaWO}_4$	$\geq 9.4 \times 10^{18}$ yr ( $0\nu 2\varepsilon$ )	[29]
$^{186}\text{W} \rightarrow ^{186}\text{Os}$	$\text{ZnWO}_4$	$\geq 2.3 \times 10^{19}$ yr ( $2\nu 2\beta^-$ )	[32]
	$^{116}\text{CdWO}_4$	$\geq 1.1 \times 10^{21}$ yr ( $0\nu 2\beta^-$ )	[45]

Large-scale scintillator-based projects to search for neutrinoless double  $\beta$  decay with sensitivity on the level of the inverted hierarchy of the neutrino masses have been proposed [46, 47, 48]. In this regard, it is of note that the SuperNEMO double  $\beta$  decay project [49] intends to utilize a large amount of plastic scintillators for the calorimeter of the detector [50].

Cryogenic scintillation bolometers (see e.g. [51, 52, 53, 54, 55]), with a typical energy resolution of a few keV and potentially with strong reduced background, look perspective technique for future  $0\nu 2\beta$  decay experiments able to explore the full range of the inverted hierarchy of the neutrino mass (half-life sensitivity on the level of  $10^{26} - 10^{28}$  years) [56, 57, 58]. At present ZnSe [59, 60, 61, 33],  $\text{Li}_2\text{MoO}_4$  [62, 35] and  $\text{CaMoO}_4$  [63, 64],  $\text{CdWO}_4$  [65, 66, 67] are considered as the most promising materials for high sensitivity scintillating-bolometers  $2\beta$  decay experiments. The large-scale experiments intend to use  $10^2 - 10^3$  kg of highly radiopure scintillators enriched in the isotopes of interest. It should be mentioned R&D of other crystal scintillators containing molybdenum:  $\text{ZnMoO}_4$  [68, 69, 35],  $\text{Li}_2\text{Zn}_2(\text{MoO}_4)_3$  [70],  $\text{Li}_2\text{Mg}_2(\text{MoO}_4)_3$  [71],  $\text{Na}_2\text{Mo}_2\text{O}_7$  [72],  $\text{Sr}_2\text{MoO}_4$  [73].

The double beta decay projects require as much as possible low, in ideal case zero, background of a detector in a region of interest<sup>1</sup>. The most dangerous radionuclides for  $2\beta$  experiments are  $^{226}\text{Ra}$  and  $^{228}\text{Th}$ , since their daughters ( $^{214}\text{Bi}$  and  $^{208}\text{Tl}$ ) have large energies of decay:  $Q_\beta = 3270$  keV and  $Q_\beta = 4999$  keV, respectively. Potassium typically contributes to the energies below 1461 keV. However,  $^{40}\text{K}$  can produce background hampering  $2\nu 2\beta$  measurements. Presence of cosmogenic radioactivity should be also controlled and decreased as much as possible. A reachable (and measurable with present instrumentation) level of a few  $\mu\text{Bq/kg}$  in crystal scintillators is discussed now (see, e.g. [68, 35, 74, 75, 76]).

## 2.2 Dark matter

There is an evidence for a large amount of invisible (dark) matter in the Universe which reveals itself only through gravitational interaction. Weakly interacting massive particles (WIMPs), in particular neutralino, predicted by the Minimal Supersymmetric extensions of the Standard Model, are one of the many possible candidates of dark matter [77, 78, 79, 80, 81]. In direct detection investigation the annual modulation signature is a powerful tool because it is independent on the nature of the dark matter candidate. It is exploited e.g. by DAMA [82] with highly radiopure NaI(Tl) crystal scintillators.

In the case of the WIMP scenarios, WIMPs can be detected due to their scattering on nuclei producing low energy nuclear recoils. An extremely low counting rate (less than several counts  $\text{kg}^{-1} \text{d}^{-1}$ ) and small energy of recoil nuclei (below 100 keV) are expected in experiments to search for the WIMPs. Direct methods of WIMP detection are based on registration of ionization, scintillation or heat release caused by recoil nucleus embedded in the material of the detector; the nucleus could be in an excited state. At present, most sensitive direct experiments apply a variety of detection techniques for WIMP search: semiconductor detectors [83, 84, 85, 86, 87], noble gases based detectors [88, 89, 90, 91, 92, 93, 94, 95], bubble chambers [96], cryogenic bolometers [97, 98, 99]. Crystal scintillators are applied in conventional scintillation detectors [100, 101, 102, 82, 103] and in cryogenic scintillating bolometers, that use simultaneous registration of heat and light signals from crystal scintillators to reject background caused by electrons [104, 105]. There are several dark matter experiments in preparation using sodium

---

<sup>1</sup>The decay energy of the most promising  $2\beta$  nuclei is  $\sim 2 - 3$  MeV.

iodine crystal scintillators as conventional room temperature scintillation detectors [106, 107, 108, 109, 110] and low-temperature scintillating bolometers [111]. Utilization of undoped CsI crystal scintillator as low-temperature scintillating bolometer is considered in Ref.[112]. High scintillation efficiency  $\text{CaI}_2$  crystal scintillators (absolute light output  $\sim 106,000$  photon/MeV) were recently proposed as WIMP detectors aiming at decreasing the energy threshold [113, 114]. Anisotropic  $\text{ZnWO}_4$  crystal scintillator is proposed to search for directionality of dark matter signals [115, 116].

Radioactive contamination of target scintillation crystals plays a key role to decrease background in the experiments. Counting rate of a few counts  $\text{kg}^{-1} \text{d}^{-1}$  in the energy interval up to  $\sim 20$  keV is typical in the present scintillator-based dark matter experiments [102, 82, 105]. The radioactive contamination of crystal scintillators used in dark matter experiments by potassium, uranium, radium, thorium and their daughters limits the experiments sensitivity. Besides, primordial ( $^{87}\text{Rb}$ ,  $^{113}\text{Cd}$ ,  $^{115}\text{In}$ ,  $^{138}\text{La}$ ,  $^{176}\text{Lu}$ ,  $^{187}\text{Re}$ ), cosmogenic (we refer reader to the review [117]) and artificial ( $^{60}\text{Co}$ ,  $^{134}\text{Cs}$ ,  $^{137}\text{Cs}$ , etc.)  $\beta$  active nuclides can produce background in scintillation dark matter experiments too. It should be stressed that presence of these radionuclides in crystals on the levels significant for dark matter experiments can be detected in practice only under extremely low background conditions with high detection efficiency (actually, in the course of dark matter experiments).

### 2.3 Measurements of neutrino fluxes

Measurements of solar and reactor neutrino fluxes allow to refine our understanding of neutrino properties, in particular, to determine parameters of the Pontecorvo-Maki-Nakagawa-Sakata matrix and to test the Mikheyev-Smirnov-Wolfenstein effect [5, 118, 119, 120]. These experiments require large-volume detectors (tens - thousands tons) with an extremely low level of radioactive contamination ( $\sim \text{nBq/kg}$ ). Especially purified liquid scintillators are used for the real-time measurements of the solar neutrino flux in the Borexino experiment [121] and to measure anti-neutrino flux from distant nuclear reactors in the KamLAND detector [122].

Low radioactive liquid scintillation detectors are used in experiments to measure antineutrino fluxes from nuclear reactors [123]. There are several projects of large scale experiments with reactor neutrinos. The Daya Bay [124], Double Chooz [125], and RENO [126] experiments utilized gadolinium-doped liquid scintillator to measure the value of the neutrino mixing angle  $\theta_{13}$ . The ambitious JUNO project intends to utilize 20 kton liquid scintillation underground detector aiming at determination of the neutrino mass hierarchy [127, 128]. It is expected that the intrinsic radiopurity of the scintillator should be better [129] to those reached in the Borexino and KamLAND detectors.

### 2.4 Search for hypothetical processes and particles

Scintillation detectors were used in a number of experiments to search for hypothetical processes beyond the Standard Model: decay of electron with violation of electric charge conservation, decay of nucleons and pairs of nucleons, charge non-conserving (CNC) beta decay, violation of the Pauli exclusion principle (PEP), search for magnetic momentum of neutrino, etc. Searches for the PEP violation were realized in [130, 131, 132] utilizing data of low background experiments with NaI(Tl) crystal scintillators. Data of the DAMA experiment have also been used to search for CNC transitions in  $^{23}\text{Na}$  and  $^{127}\text{I}$  nuclei [133], searches for nucleons decay to invisible

channels [134], instability of electron [131, 135], solar axions [136]. Large mass and ultra-low level of radioactive background of the Borexino detector have allowed to establish new limits on processes of decay of nucleons into invisible channels (for example, with emission of only neutrinos) [137], on magnetic momentum of neutrino [138], to search for solar axions [139, 140] and for the PEP violation [141]. Invisible nucleons decays were searched for also in the SNO and KamLAND experiments [142, 143]. In work [144] search for activity with electric charge non-conservation was realized in the experiment with  $\text{LaCl}_3(\text{Ce})$  crystal scintillator.

## 2.5 Investigation of rare $\alpha$ and $\beta$ decays

Crystal scintillators, both as ordinary scintillation detectors and as cryogenic scintillating bolometers, are successfully used to investigate rare  $\alpha$  and  $\beta$  decays. The half-life and the spectrum shape of the fourth-forbidden  $\beta$  decay of  $^{113}\text{Cd}$  were measured with the help of  $\text{CdWO}_4$  crystal scintillators [145, 146, 147]. In the experiment [147] the  $^{113}\text{Cd}$  half-life was determined with the highest to-date accuracy  $T_{1/2} = (8.04 \pm 0.05) \times 10^{15}$  yr. Liquid scintillators were used to measure shape of spectrum and half-life of long-lived isotopes  $^{87}\text{Rb}$  ( $T_{1/2} = 4.967(32) \times 10^{10}$  yr [148]) and  $^{115}\text{In}$  ( $T_{1/2} = 4.41(26) \times 10^{14}$  yr [149]). Recently  $\text{YVO}_4$  scintillating bolometer was identified as a promising tool for investigation of rare ( $T_{1/2} \simeq 10^{17}$  yr)  $\beta^-$  and EC decays of  $^{50}\text{V}$  [150]. In 1960 Beard and Kelly have utilized small  $\text{CaWO}_4$  and  $\text{CdWO}_4$  crystals in low background experiments to search for alpha activity of natural tungsten [151]. However, even more sensitive experiment with  $\text{CdWO}_4$  crystal scintillator did not allow to observe  $\alpha$  decays of tungsten [152]. The first indication on the decay of  $^{180}\text{W}$  with a half-life  $T_{1/2} = 1.1 \times 10^{18}$  yr was obtained with the help of enriched  $^{116}\text{CdWO}_4$  crystal scintillator [153]. This observation was confirmed with  $\text{CaWO}_4$  crystals (as cryogenic scintillating bolometer [154] and room temperature scintillation detector [155]) and  $\text{ZnWO}_4$  crystal scintillator [156]. The alpha activity of bismuth ( $^{209}\text{Bi}$ , considered before as the heaviest stable element in the nature) with the half-life  $T_{1/2} = (1.9 \pm 0.2) \times 10^{19}$  yr has been detected with the help of BGO cryogenic scintillator [157]. In the same approach, decay of  $^{209}\text{Bi}$  to the first excited level of  $^{205}\text{Tl}$  was also observed [158]. An indication on rare  $\alpha$  activity of natural europium ( $^{151}\text{Eu}$ ) obtained in the low background experiment by using  $\text{CaF}_2(\text{Eu})$  crystal scintillator [159] was confirmed with  $\text{Li}_6\text{Eu}(\text{BO}_3)_3$  crystal scintillator operated as a scintillating bolometer [160]. Half-life limits on  $\alpha$  decays of Pb isotopes were obtained with  $\text{PbWO}_4$  scintillating bolometer grown from ancient Roman lead with low  $^{210}\text{Pb}$  activity [161].  $\text{ZnWO}_4$  scintillating bolometer doped with enriched  $^{148}\text{Sm}$  was used for more precise measurement of  $^{148}\text{Sm}$  half-life as  $T_{1/2} = 6.4_{-1.3}^{+1.2} \times 10^{15}$  yr [162]. An interesting study of the L/K electron capture ratio in the decay of  $^{207}\text{Bi}$  decay to the 1633 keV excited level of  $^{207}\text{Pb}$  was realized with a BGO scintillating bolometer contaminated by  $^{207}\text{Bi}$  [163]. Rare (probability of  $\sim 10^{-9}$ ) emission of  $e^+e^-$  pairs in  $\alpha$  decay of  $^{241}\text{Am}$  was measured with  $\text{NaI}(\text{Tl})$  scintillators in Ref. [164].

## 3 Experimental methods to measure radioactive contamination of scintillators

Methods of determination of radioactive contaminants in scintillators could be classified as direct, when characteristic radioactivity of specific isotope is detected, and indirect, which give quantitative conclusion on the presence of specific isotope on the basis of measurements of

contamination by the corresponding chemical element (by mass-spectrometry or fluorescence methods) or its daughters (by neutron activation analysis). The main characteristics of elements containing primordial radioactive isotopes are presented in Table 2. While indirect methods can be applied to any material, scintillators can measure their own internal radioactive contamination by themselves. This provides in general higher sensitivity, and further we will give more details on methods of analysis of radioactive contaminants in the data collected with scintillators.

Table 2: Elements containing primordial radioactive isotopes (except radium that is originated from  $^{238}\text{U}$  decay). Data on the half-lives of  $\alpha$  and  $\beta$  active isotopes are taken from [165] if other source is not referred; year is accepted as  $1 \text{ yr} = 365.2422 \text{ d}$ ; the isotopic abundances are from [166] (the abundance of  $^{226}\text{Ra}$  is assumed to be 100%); the atomic weights are from [167].

Element	Radioactive isotope, decay modes	Isotopic abundance	Half-life (yr)	Activity in 1 g of element (Bq)	Mass of element (g) corresponding to 1 mBq activity of the radioactive isotope
Potassium	$^{40}\text{K}$ , $\varepsilon$ , $\beta^-$	0.000117(1)	$1.248(3) \times 10^9$	31.7(3)	$3.15(3) \times 10^{-5}$
Calcium	$^{48}\text{Ca}$ , $2\beta^-$	0.00187(21)	$6.4_{-1.1}^{+1.4} \times 10^{19}$ [168]	$10(2) \times 10^{-9}$	$1.0(3) \times 10^5$
Vanadium	$^{50}\text{V}$ , $\varepsilon$	0.00250(10)	$2.29(25) \times 10^{17}$ [169]	$2.8(3) \times 10^{-6}$	352(40)
Germanium	$^{76}\text{Ge}$ , $2\beta^-$	0.0775(12)	$1.926(94) \times 10^{21}$ [170]	$7.1(4) \times 10^{-9}$	$1.41(7) \times 10^5$
Selenium	$^{82}\text{Se}$ , $2\beta^-$	0.0882(15)	$9.6(10) \times 10^{19}$ [171]	$1.5(2) \times 10^{-7}$	$6.5(7) \times 10^3$
Rubidium	$^{87}\text{Rb}$ , $\beta^-$	0.2783(2)	$4.97(3) \times 10^{10}$	867(5)	$1.154(7) \times 10^{-6}$
Zirconium	$^{96}\text{Zr}$ , $2\beta^-$	0.0280(2)	$2.35(21) \times 10^{19}$ [172]	$1.73(15) \times 10^{-7}$	$5.8(5) \times 10^3$
Molybdenum	$^{100}\text{Mo}$ , $2\beta^-$	0.09744(65)	$6.9(4) \times 10^{18}$ [35]	$1.95(11) \times 10^{-6}$	514(31)
Cadmium	$^{113}\text{Cd}$ , $\beta^-$	0.12227(7)	$8.04(5) \times 10^{15}$	$1.789(11) \times 10^{-3}$	0.559(4)
	$^{116}\text{Cd}$ , $2\beta^-$	0.07512(54)	$2.69(14) \times 10^{19}$ [41]	$3.28(17) \times 10^{-7}$	$3.05(16) \times 10^3$
Indium	$^{115}\text{In}$ , $\beta^-$	0.95719(52)	$4.41(25) \times 10^{14}$	0.250(14)	$4.00(23) \times 10^{-3}$
Tellurium	$^{128}\text{Te}$ , $2\beta^-$	0.3174(8)	$2.0(3) \times 10^{24}$ [173]	$1.65(25) \times 10^{-11}$	$6.1(9) \times 10^7$
	$^{130}\text{Te}$ , $2\beta^-$	0.3408(62)	$8.2(6) \times 10^{20}$ [174]	$4.3(3) \times 10^{-8}$	$2.32(19) \times 10^4$
Lanthanum	$^{138}\text{La}$ , $\varepsilon$ , $\beta^-$	0.0008881(71)	$1.03(1) \times 10^{11}$	0.821(11)	$1.218(15) \times 10^{-3}$
Neodymium	$^{144}\text{Nd}$ , $\alpha$	0.23798(19)	$2.29(16) \times 10^{15}$	$9.5(7) \times 10^{-3}$	0.105(7)
	$^{150}\text{Nd}$ , $2\beta^-$	0.05638(28)	$9.34_{-0.64}^{+0.66} \times 10^{18}$ [175]	$5.5(4) \times 10^{-7}$	$1.81(13) \times 10^3$
Samarium	$^{147}\text{Sm}$ , $\alpha$	0.1500(14)	$1.060(11) \times 10^{11}$	124.5(18)	$8.03(11) \times 10^{-6}$
	$^{148}\text{Sm}$ , $\alpha$	0.1125(9)	$6.4_{-1.3}^{+1.2} \times 10^{15}$ [162]	$1.5(3) \times 10^{-3}$	0.65(13)
Europium	$^{151}\text{Eu}$ , $\alpha$	0.4781(6)	$4.6(1.2) \times 10^{18}$ [160]	$9.0(24) \times 10^{-6}$	111(29)
Gadolinium	$^{152}\text{Gd}$ , $\alpha$	0.0020(3)	$1.08(8) \times 10^{14}$	$1.56(27) \times 10^{-3}$	0.64(10)
Lutetium	$^{176}\text{Lu}$ , $\beta^-$	0.02599(13)	$3.640(35) \times 10^{10}$ [176]	54.0(6)	$1.853(20) \times 10^{-5}$
Hafnium	$^{174}\text{Hf}$ , $\alpha$	0.0016(12)	$2.0(4) \times 10^{15}$	$6(5) \times 10^{-5}$	17(13)
Tungsten	$^{180}\text{W}$ , $\alpha$	0.0012(1)	$1.8(2) \times 10^{18}$ [154]	$4.8(5) \times 10^{-8}$	$2.08(23) \times 10^4$
Rhenium	$^{187}\text{Re}$ , $\beta^-$	0.6260(5)	$4.33(7) \times 10^{10}$	1027(17)	$9.74(16) \times 10^{-7}$
Osmium	$^{186}\text{Os}$ , $\alpha$	0.0159(64)	$2.0(11) \times 10^{15}$	$6(4) \times 10^{-4}$	1.8(12)
Platinum	$^{190}\text{Pt}$ , $\alpha$	0.00012(2)	$4.97(16) \times 10^{11}$ [177]	0.0164(29)	0.061(10)
Bismuth	$^{209}\text{Bi}$ , $\alpha$	1	$2.01(8) \times 10^{19}$	$3.15(13) \times 10^{-6}$	318(13)
Radium	$^{226}\text{Ra}$ , $\alpha$	1	1600(7)	$3.658(16) \times 10^{10}$	$2.734(12) \times 10^{-14}$
Thorium	$^{230}\text{Th}$ , $\alpha$	0.0002(2)	$7.54(3) \times 10^4$	$1.5(15) \times 10^5$	$6.6(66) \times 10^{-9}$
	$^{232}\text{Th}$ , $\alpha$	0.9998(2)	$1.40(1) \times 10^{10}$	4071(29)	$2.456(18) \times 10^{-7}$
Uranium	$^{234}\text{U}$ , $\alpha$	0.000054(5)	$2.455(6) \times 10^5$	$1.22(12) \times 10^4$	$8.2(7) \times 10^{-8}$
	$^{235}\text{U}$ , $\alpha$	0.007204(6)	$7.04(1) \times 10^8$	568.7(9)	$1.7585(29) \times 10^{-6}$
	$^{238}\text{U}$ , $\alpha$	0.992742(10)	$4.468(6) \times 10^9$	12347(17)	$8.099(11) \times 10^{-8}$

## 3.1 Indirect methods

Long living radioactive isotopes can be measured with the help of Inductively Coupled Plasma Mass Spectrometry (ICP-MS). Sensitivity of this method depends on measured matrix and on previous use of an apparatus. For instance, sensitivity of the spectrometers installed in the Gran Sasso underground laboratory of I.N.F.N. (Italy) to the solids and reagents involved in the  $\text{TeO}_2$  crystals production process was on the level of  $\sim (2 \times 10^{-10} - 2 \times 10^{-12})$  g/g for  $^{232}\text{Th}$  and  $^{238}\text{U}$  [178], which corresponds to activity of  $^{232}\text{Th}$  and  $^{238}\text{U}$ :  $\sim (0.8 - 0.008)$  mBq/kg and  $\sim (2 - 0.02)$  mBq/kg, respectively. Sensitivity of ICP-MS method to potassium is hampered due to interference of  $^{39}\text{K}$  with polyatomic species produced from argon used in the plasma source of ICP-MS devices [178]. The measured  $^{39}\text{K}$  concentrations in NaI powder for radiopure NaI(Tl) crystal scintillators production were  $\sim (1 \times 10^{-8} - 2 \times 10^{-7})$  g/g, while the detection limit was on the level of  $< 3 \times 10^{-9}$  g/g [178], that corresponds to  $^{40}\text{K}$  activity  $\sim (0.3 - 6)$  mBq/kg and a detection limit  $< 0.09$  mBq/kg. A higher sensitivity (a detection limit 0.016 mBq/kg of  $^{40}\text{K}$  in NaI matrix) was reported in [179]. The improved sensitivity was achieved thanks to the use of improved instrumentation, cool plasma operating conditions, and meticulously clean sample preparations. Accelerator mass-spectrometry allows to reach much higher sensitivity up to  $\sim 10^{-17}$  g/g (potassium in liquid scintillator [180]). Unfortunately, mass-spectrometry is practically useless to measure contamination by  $^{226}\text{Ra}$  (daughter of  $^{238}\text{U}$ ) and  $^{228}\text{Th}$  ( $^{232}\text{Th}$ ) due to the rather short half-lives of these isotopes. At the same time, activities of these radionuclides (those daughters,  $^{214}\text{Bi}$  and  $^{208}\text{Tl}$ , are the most unfavorable background sources for double  $\beta$  decay experiments) can be substantially different from  $^{238}\text{U}$  and  $^{232}\text{Th}$  due to broken secular equilibrium. The same can be said about  $^{210}\text{Pb}$ , daughter of  $^{238}\text{U}$ , one of the most troublesome contaminant radionuclides for dark matter experiments.

A very high sensitivity to  $^{40}\text{K}$ ,  $^{232}\text{Th}$  and  $^{238}\text{U}$  on the level of nBq/kg was reached by using neutron-activation technique to measure contamination of liquid scintillator for the KamLAND experiment [181]. While neutron-activation analysis is very powerful tool to measure radioactive contamination in organic scintillators, the method is much less effective to examine inorganic materials due to possible activation of scintillation crystals matrix [182]. Comparison of the most sensitive indirect methods (mass spectrometry and neutron activation technique) with direct counting is discussed in [183].

It should be stressed that the various analytical methods used for analysis of chemical impurities in raw materials for crystal growth, like for instance Atomic Absorption Spectroscopy, X-ray Fluorescence, allow to estimate presence of long-living naturally occurring primordial radioactive elements too. It is worth to mention also Electron Microscope measurements to estimate presence of platinum in  $^{116}\text{CdWO}_4$  crystal scintillators [153]. However, the sensitivity of these methods are much below of the ICP-MS sensitivity, not to say for direct counting methods [182, 184].

## 3.2 Direct detection

### 3.2.1 Low background measurements

Ultra-low background HP Ge  $\gamma$  detectors can be used to measure radioactive contamination of scintillation crystals and materials for their production (see, for instance [185, 186, 191, 192, 193, 194, 195, 196, 197, 198, 187, 188, 189, 190]). This method provides typical sensitivity at the level of mBq/kg for  $^{40}\text{K}$ ,  $^{137}\text{Cs}$ ,  $^{228}\text{Th}$ ,  $^{226}\text{Ra}$  and  $^{227}\text{Ac}$  (daughter of  $^{235}\text{U}$ ), and somewhat

lower sensitivity to other U/Th daughters. However, this approach is useless to detect internal contamination by  $\alpha$  and  $\beta$  active isotopes if decay goes to the ground state of a daughter nucleus<sup>2</sup>.

The highest sensitivity to measure internal contamination of scintillators can be achieved in low background measurements where the scintillator is operating as a detector. Such an approach provides high detection efficiency, especially for  $\alpha$  and  $\beta$  particles. A typical low background scintillation set-up (see, for instance, [199, 200, 201, 202, 203, 44, 204, 205, 206, 207, 208, 209, 41]) consists of scintillator, light-guide to shield the scintillator from radioactivity of photomultiplier tubes (typically, the most contaminated details of a low background scintillation set-up), passive shield. Background of the detector can be further suppressed by using of active shield counters surrounding the main detector, and anti-muon veto counters[45, 195]. Light-guides made of a scintillation material with different (relative to the main scintillation detector) scintillation decay time can serve as active anticoincidence detectors [45, 195, 38]. Continuous flushing of internal volume of a set-up by a radon-free gas (typically by nitrogen) allows to reduce background caused by radon [205, 209]. It is worth mentioning a possibility to reduce background further by using data on time of arrival and pulse-shape of scintillation signals (the methods will be considered in Sections 3.2.3 and 3.2.4).

Below we will discuss response of a scintillation detector to  $\gamma$  quanta,  $\beta$  and  $\alpha$  particles, pulse-shape discrimination, time-amplitude analysis, Monte-Carlo simulation of background components. These methods allow to describe background energy spectra accumulated with a scintillation counter and estimate radioactive contamination of the scintillator.

### 3.2.2 Response of scintillation detector to $\gamma$ quanta, $\beta$ and $\alpha$ particles

Knowledge of a detector response to  $\gamma$  quanta (response function, dependence of energy resolution on energy) and  $\alpha$  particles (energy dependence of  $\alpha/\beta$  ratio<sup>3</sup> and energy resolution) is necessary to interpret background of the detector.

Response function and dependence of energy resolution on energy of  $\gamma$  quanta can be measured with  $\gamma$  sources in a wide energy interval from a few keV (5.9 keV Mn K X-rays from <sup>55</sup>Fe) up to 2615 keV ( $\gamma$  quanta of <sup>208</sup>Tl). Calibration with  $\alpha$  sources is much more complicated task because energies of commonly used  $\alpha$  sources lie in the energy region from  $\sim 5.3$  to  $\sim 8.8$  MeV (<sup>228</sup>Th, <sup>241</sup>Am, <sup>244</sup>Cm, <sup>252</sup>Cf). To calibrate detector at lower energies,  $\alpha$  sources with absorbers can be used (see, for instance [153, 205, 155, 210, 159]). Response of scintillation detectors to  $\alpha$  particles is non-linear. An example of  $\alpha/\beta$  ratio dependence on energy is shown in Fig. 1, where the  $\alpha/\beta$  ratio measured with a CaWO<sub>4</sub> crystal scintillator is presented. As the quenching of the scintillation light caused by  $\alpha$  particles is due to the higher ionization density, such a behavior of the  $\alpha/\beta$  ratio can be explained by the energy dependence of ionization density of particles [211, 212]. See recent review [213] on  $\alpha/\beta$  ratio in different scintillators.

Alpha peaks from internal contamination of scintillators allow to extend the interval of  $\alpha$  particles energies (see Fig. 1 and Fig. 2). In addition,  $\alpha$  peaks from internal contamination provide an important test of calibration measurements with external sources. It should be

---

<sup>2</sup>Beta activity can be detected by HP Ge detectors via registration of bremsstrahlung, however the sensitivity in this case is much lower due to low efficiency and absence of a clear signature (like peaks in  $\gamma$  spectra).

<sup>3</sup>Here we define the “ $\alpha/\beta$  ratio” as the ratio of  $\alpha$  peak position measured in the  $\gamma$  energy scale to the energy of  $\alpha$  particles. As usual, a detector energy scale is measured with  $\gamma$  sources, thus the notation “ $\alpha/\gamma$  ratio” is more adequate. However, because  $\gamma$  rays interact with matter by means of the energy transfer to electrons, in the present paper we are using a more traditional term “ $\alpha/\beta$  ratio”.

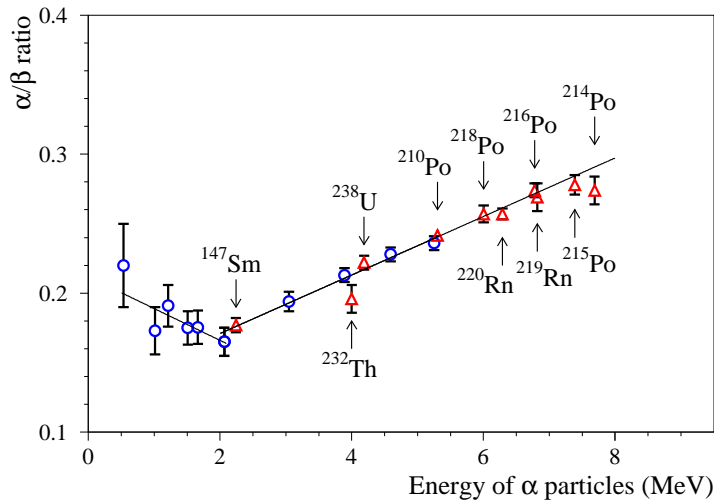


Figure 1: The energy dependence of the  $\alpha/\beta$  ratio measured with  $\text{CaWO}_4$  crystal scintillator [155]. The points obtained by irradiation of the scintillator by external  $\alpha$  particles are shown by circles, while the points obtained by analysis of  $\alpha$  peaks from the internal contamination of the crystal by  $\alpha$  active nuclides are drawn by triangles.

stressed that analysis of internal  $\alpha$  peaks is only practical method to measure response to  $\alpha$  particles for encapsulated scintillation detectors produced from highly hygroscopic materials, like  $\text{NaI}(\text{Tl})$ ,  $\text{LaCl}_3(\text{Ce})$ ,  $\text{LaBr}_3$ , etc.

In some scintillation crystals with anisotropic structure,  $\alpha/\beta$  ratio depends on the direction of  $\alpha$  particles relatively to crystal axes. Such an effect was observed in anthracene [214], stilbene [215], and  $\text{CdWO}_4$  [153],  $\text{ZnWO}_4$  [210], and  $\text{MgWO}_4$  [216] crystal scintillators (see Fig. 2 where dependence of  $\alpha/\beta$  ratio on direction of  $\alpha$  irradiation relatively to crystal axes of  $\text{CdWO}_4$  scintillator is presented). It leads to some worsening of energy resolution of these detectors to  $\alpha$  particles [153, 32].

Scintillation signals for  $\gamma$  quanta can be quenched in comparison to  $\beta$  particles. E.g. there is an indication of scintillation light-efficiency quenching in  $\text{CdWO}_4$  scintillator for  $\gamma$  quanta in comparison to electrons that resulted in a higher  $Q_\beta$  value of  $^{113}\text{Cd}$  [146, 147]:  $Q_\beta = 337$  keV and  $Q_\beta = 345$  keV, respectively. These values are substantially larger than the Table value  $Q_\beta = 323.83(27)$  keV [217]. The quenching can be explained by the non-proportionality in the scintillation response of  $\text{CdWO}_4$  crystal scintillators significant for energies below  $\sim 0.1$  MeV [218]. Because of distribution of  $\gamma$  quanta energy between two and more electrons (due to the multiple Compton scattering),  $\gamma$  peaks should be shifted to lower energies in “electron” energy scale<sup>4</sup>. Organic scintillators, particularly liquid scintillators, have significant non-proportionality of scintillation response. The effect was observed in liquid scintillators used for neutrino experiments Borexino [221] and Double Chooz [222]. The effect of  $\gamma$  peaks shift in liquid scintillators is significant: e.g. the position of the 1461 keV  $\gamma$  peak of  $^{40}\text{K}$  in the scintillator used in the Borexino detector is shifted to 1360 keV relatively to the energy deposited for electrons [137].

<sup>4</sup>This effect also leads to worse energy resolution of scintillation detectors for  $\gamma$  quanta [219, 220].

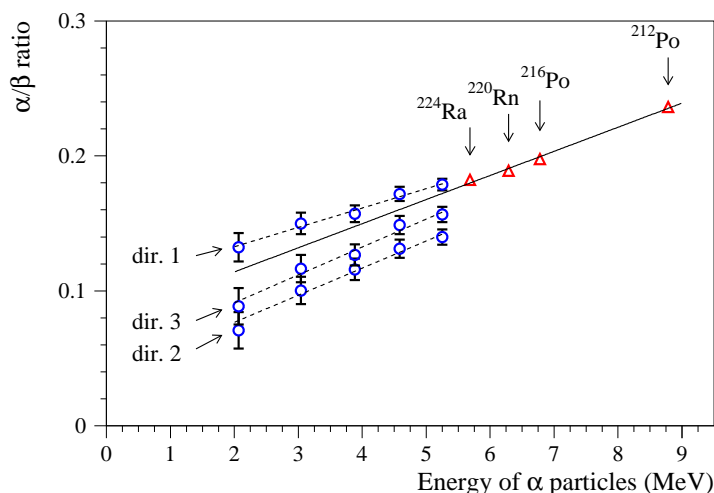
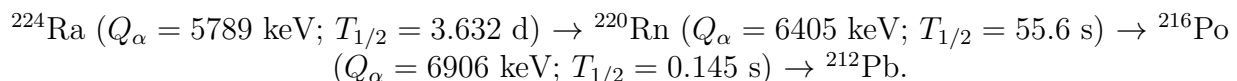


Figure 2: Energy dependence of the  $\alpha/\beta$  ratio on energy measured with  $^{116}\text{CdWO}_4$  crystal scintillator. The  $\alpha/\beta$  ratio depends on direction of irradiation relatively to crystal axes denoted as dir. 1 (along to the crystal axis [010]), dir. 2 ([001]) and dir. 3 ([100]) [153]. The points obtained by irradiation of the scintillator by external  $\alpha$  particles in the directions parallel to the axes of the crystal are shown by circles, while the points obtained by analysis of  $\alpha$  peaks from internal contamination of the scintillator by  $\alpha$  active nuclides are drawn by triangles.

### 3.2.3 Time-amplitude analysis

Data on the energy and arrival time of events can be used to select fast decay chains from the  $^{232}\text{Th}$ ,  $^{235}\text{U}$  and  $^{238}\text{U}$  families. The method of time-amplitude analysis is described in detail in [223, 224, 44, 45, 208]. For instance, the following sequence of  $\alpha$  decays from the  $^{232}\text{Th}$  family can be selected:



These radionuclides are in equilibrium with  $^{228}\text{Th}$  ( $^{232}\text{Th}$  family). As an example, the results of the time-amplitude analysis of data accumulated in the low background experiment to search for  $2\beta$  decay of  $^{116}\text{Cd}$  with the help of  $^{116}\text{CdWO}_4$  crystal scintillators are shown in Fig. 3. The obtained  $\alpha$  peaks (the  $\alpha$  nature of events was confirmed by the pulse-shape analysis described in Section 3.2.4) as well as the distributions of the time intervals between events, are in a good agreement with those expected for the  $\alpha$  decays of the  $^{224}\text{Ra} \rightarrow ^{220}\text{Rn} \rightarrow ^{216}\text{Po} \rightarrow ^{212}\text{Pb}$  chain.

Similarly the following fast sequence of  $\beta$  and  $\alpha$  decays:



(in equilibrium with  $^{226}\text{Ra}$  from the  $^{238}\text{U}$  family) can also be selected with the help of time-amplitude analysis. In Fig. 4 one can see the energy spectra and time distributions of the sequence selected from the data accumulated in the low background experiment to search for  $2\beta$  decay of  $^{160}\text{Gd}$  with the help of gadolinium orthosilicate ( $\text{Gd}_2\text{SiO}_5:\text{Ce}$ , GSO) scintillator [44]. In addition, Fig. 4 illustrates a possibility to detect another short chain:

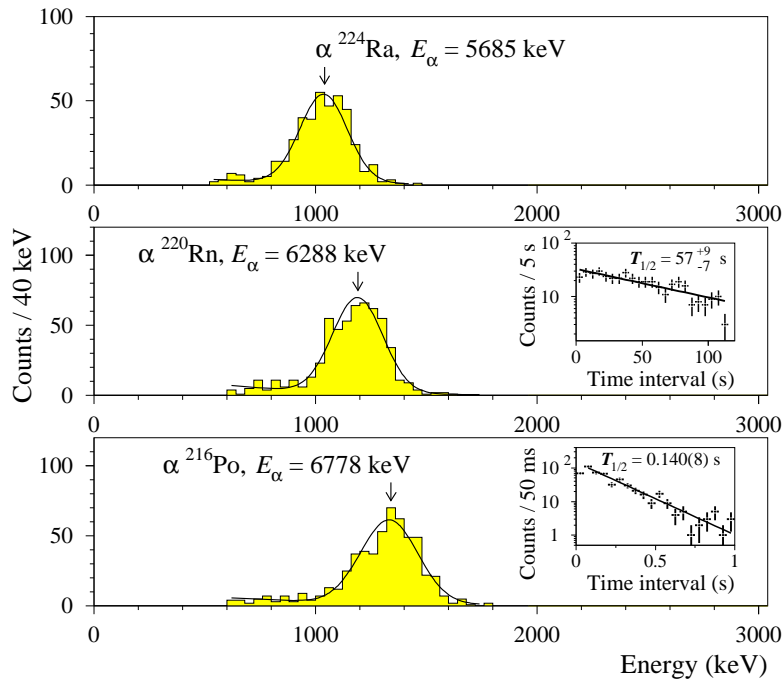


Figure 3: The  $\alpha$  peaks of  $^{224}\text{Ra}$ ,  $^{220}\text{Rn}$ , and  $^{216}\text{Po}$  selected by the time-amplitude analysis from the data accumulated during 14745 h with  $^{116}\text{CdWO}_4$  detector [153]. (Insets) The time distributions between the first and second (and between second and third) events are presented together with exponential fits. Obtained half-lives of  $^{220}\text{Rn}$  and  $^{216}\text{Po}$  ( $57^{+9}_{-7}$  s and 0.140(8) s, respectively) are in a good agreement with the table values (55.6(1) s and 0.145(2) s, respectively [165]).

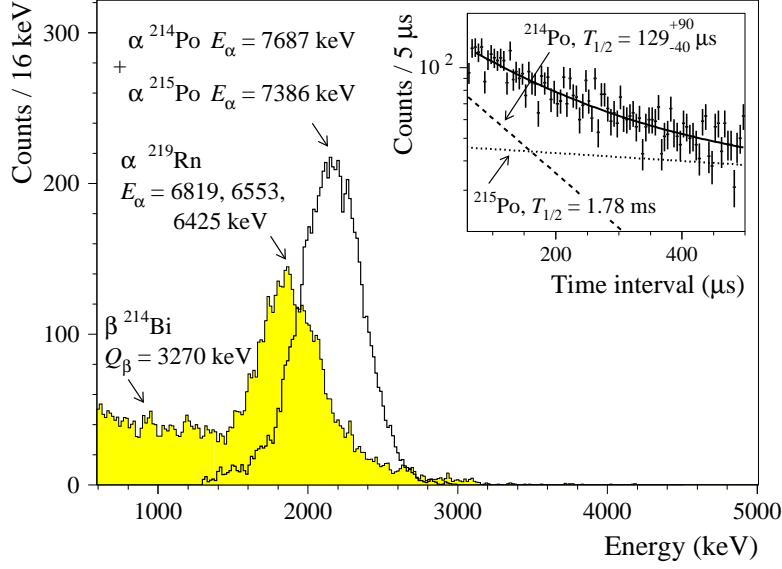


Figure 4: The energy spectra of the sequence of  $\beta$  and  $\alpha$  decays in the decay chain  $^{214}\text{Bi} \rightarrow ^{214}\text{Po} \rightarrow ^{210}\text{Pb}$  ( $^{238}\text{U}$  family) which were selected with the help of the time-amplitude analysis of 8609 h data accumulated with GSO scintillator [44]. The peak with the energy in  $\gamma$  scale  $\approx 1.8$  MeV is related with the decays of  $^{219}\text{Rn}$  from the chain  $^{219}\text{Rn} \rightarrow ^{215}\text{Po} \rightarrow ^{211}\text{Pb}$  ( $^{235}\text{U}$  family). In the insert: the distribution of the time intervals between the first and second events together with its fit (solid line) by the sum of exponent with  $T_{1/2} = 129^{+90}_{-40} \mu\text{s}$  (a table  $^{214}\text{Po}$  value is  $T_{1/2} = 164.3 \mu\text{s}$ ; dashed line) and exponent with  $T_{1/2} = 1.78$  ms corresponding to decays of  $^{215}\text{Po}$  from the chain  $^{219}\text{Rn} \rightarrow ^{215}\text{Po} \rightarrow ^{211}\text{Pb}$  (dotted line).



Radionuclide  $^{219}\text{Rn}$  is in equilibrium with  $^{227}\text{Ac}$  from the  $^{235}\text{U}$  family. In this case the events of  $^{214}\text{Po}$  and  $^{215}\text{Po}$  decays are superimposed (see Fig. 4). Nevertheless activities of  $^{226}\text{Ra}$  and  $^{227}\text{Ac}$  can be calculated separately thanks to possibility to distinguish between the broad  $\beta$  spectrum of  $^{214}\text{Bi}$  and  $\alpha$  peak of  $^{219}\text{Rn}$ .

### 3.2.4 Pulse-shape discrimination

Most of scintillators have slightly different decay kinetic for  $\beta$  particles ( $\gamma$  quanta) and  $\alpha$  particles. It allows to discriminate these particles, and therefore, to estimate activity of  $\alpha$  and  $\beta$  active nuclides separately. Different methods can be used to realize pulse-shape discrimination. We would like to refer to the optimal filter method proposed by Gatti and De Martini [225], and developed in [226] for  $\text{CdWO}_4$  crystal scintillators, and then successfully applied to many scintillators [205, 229, 210, 153, 155, 159, 227, 228, 216]. In the optimal filter method, a shape indicator ( $SI$ ) - a numerical characteristic - can be calculated for each scintillation event produced by a scintillator:

$$SI = \frac{\sum [f(t_k) \times P(t_k)]}{\sum f(t_k)}, \quad (1)$$

where the sum is over time channels  $k$  from the origin of the pulse up to a certain time;  $f(t_k)$

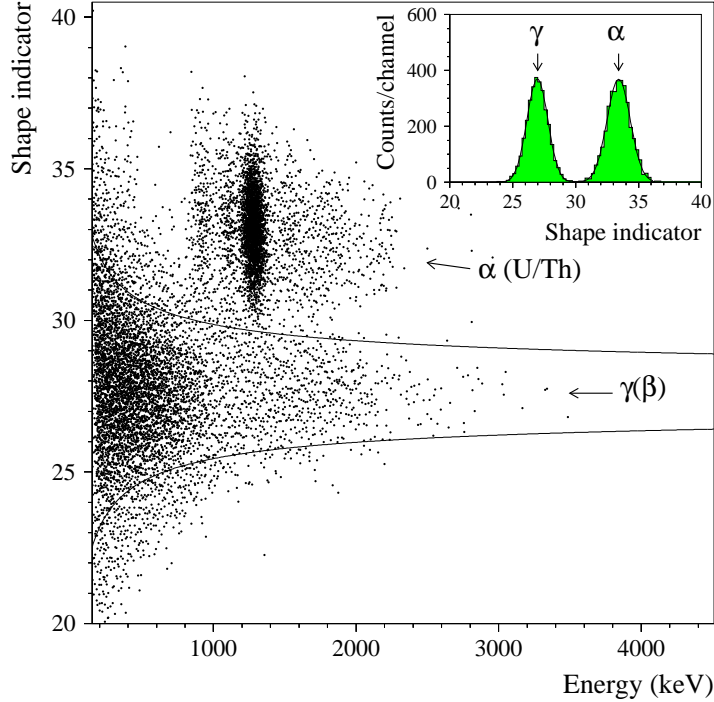


Figure 5: Scatter plot of the shape indicator  $SI$  (see text) versus energy for 171 h of the background data measured with  $\text{CaWO}_4$  crystal scintillator. Lines show  $\pm 2\sigma$  region of  $SI$  for  $\gamma(\beta)$  events. (Inset) The  $SI$  distributions measured in calibration runs with  $\alpha$  particles ( $E_\alpha = 5.3$  MeV) and  $\gamma$  quanta ( $\approx 1.2$  MeV) [230].

is the digitized amplitude of the signal (at the time  $t_k$ ). The weight function  $P(t_k)$  is defined as:

$$P(t_k) = [f_\alpha(t_k) - f_\gamma(t_k)]/[f_\alpha(t_k) + f_\gamma(t_k)], \quad (2)$$

where  $f_\alpha(t_k)$  and  $f_\gamma(t_k)$  are the reference pulse shapes for  $\alpha$  particles and  $\gamma$  quanta. To realize the optimal filter method, the pulse shapes for  $\alpha$  particles and  $\gamma$  quanta should be studied. The distributions of the shape indicators have Gaussian shape. Therefore, the figure of merit ( $FOM$ ) – a measure of discrimination ability – can be calculated using the following expression proposed by Gatti and De Martini:

$$FOM = |SI_\alpha - SI_\gamma|/\sqrt{\sigma_\alpha^2 + \sigma_\gamma^2}. \quad (3)$$

One can see an illustration of pulse-shape discrimination by using the optimal filter method in Fig. 5 where the scatter plot of the shape indicator versus energy is shown for the data measured with a  $\text{CaWO}_4$  crystal scintillator [230]. Energy spectrum of  $\alpha$  events selected from the data measured with the  $\text{CaWO}_4$  crystal over 1734 h is presented in Fig. 6, while an energy spectrum of  $\beta(\gamma)$  events is shown in Fig. 7.

The mean time method is also widely used to discriminate  $\beta(\gamma)$  and  $\alpha$  particles in scintillation detectors (see e.g. [187, 202, 208, 228]). The following formula can be applied to calculate the mean time parameter  $\langle t \rangle$  for each pulse:

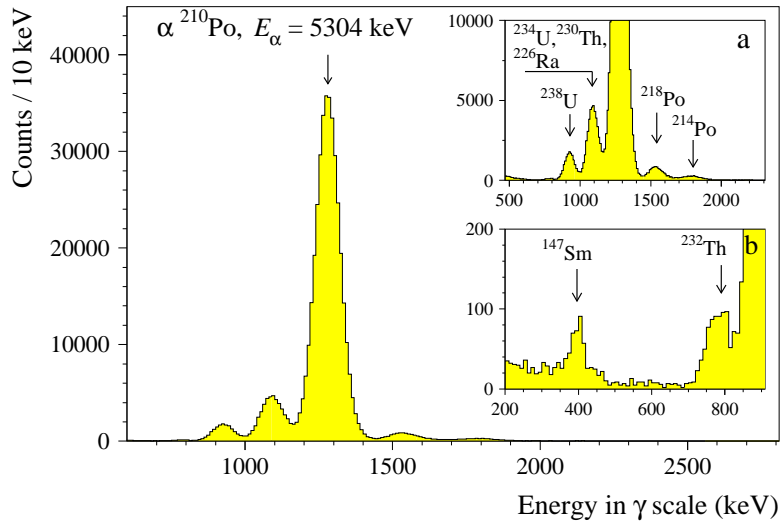


Figure 6: Energy spectrum of  $\alpha$  events selected by the pulse-shape analysis from background data measured over 1734 h with  $\text{CaWO}_4$  detector [230]. (Inset a) The same spectrum but scaled up. It is well reproduced by the model, which includes  $\alpha$  decays of nuclides from  $^{232}\text{Th}$  and  $^{238}\text{U}$  families. (Inset b) Low energy part of the spectrum where an  $\alpha$  peak of  $^{147}\text{Sm}$  is clearly visible.

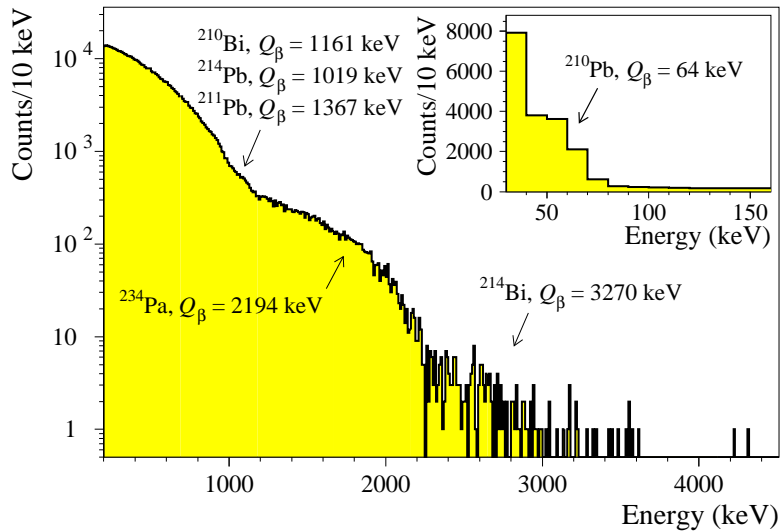


Figure 7: Energy spectrum of  $\beta(\gamma)$  events selected by the pulse-shape analysis technique from the background data measured over 1734 h with  $\text{CaWO}_4$  detector [230]. The distribution is described by the  $\beta$  spectra of  $^{210}\text{Bi}$ ,  $^{214}\text{Pb}$ ,  $^{211}\text{Pb}$ ,  $^{234m}\text{Pa}$ , and  $^{214}\text{Bi}$ . (Inset) In the low energy region, the background (measured over 15.8 h) is caused mainly by decay of  $^{210}\text{Pb}$ .

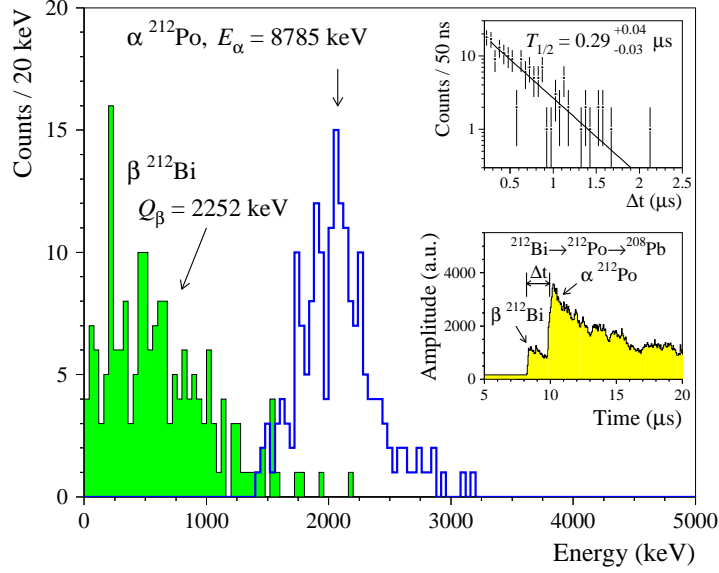


Figure 8: The energy distributions for the fast sequence of  $\beta$  ( $^{212}\text{Bi}$ ,  $Q_\beta = 2252$  keV) and  $\alpha$  ( $^{212}\text{Po}$ ,  $E_\alpha = 8785$  keV,  $T_{1/2} = 0.299$  s) decays selected by the pulse-shape analysis from the background data obtained in the experiment with cadmium tungstate crystal scintillators [153]. (Upper inset) The time distribution of intervals ( $\Delta t$ ) between  $\beta$  and  $\alpha$  signals. (Lower inset) Example of such an event in the  $\text{CdWO}_4$  scintillator.

$$\langle t \rangle = \sum (f(t_k) \times t_k) / \sum f(t_k), \quad (4)$$

where the sum is over time channels  $k$ , starting from the origin of pulse and up to a certain time. The distributions of parameters  $\langle t \rangle$  for  $\alpha$  and  $\beta(\gamma)$  signals are also well described by Gaussian functions. Thus, the same measure ( $FOM$ , see Equation 3) can be used to estimate efficiency of the method. The optimal filter method provides slightly better pulse-shape discrimination in comparison with the mean time technique (see e.g. [228]). However, the mean time method is easier to apply because it does not require the construction of a weight function, which requires knowledge of scintillation signals pulse-shape.

It should be stressed that the pulse-shape of scintillation signals for  $\alpha$  particles depends on energy. In some scintillators with anisotropic properties pulse-shape also depends on direction of  $\alpha$  irradiation relatively to the crystal axes. As in the case with the  $\alpha/\beta$  ratio, such a dependence was observed in  $\text{CdWO}_4$  [153],  $\text{ZnWO}_4$  [210], and  $\text{MgWO}_4$  [216] crystal scintillators.

Pulse-shape analysis can also be applied to the very fast sequence of decays from the  $^{232}\text{Th}$  family:



An example of such an analysis is presented in Fig. 8, where the  $\beta$  spectrum of  $^{212}\text{Bi}$ , the  $\alpha$  peak of  $^{212}\text{Po}$  and the distribution of the time intervals between the first and the second pulses selected from the data of low background experiment [153] are depicted. This method is more effective with fast scintillators.

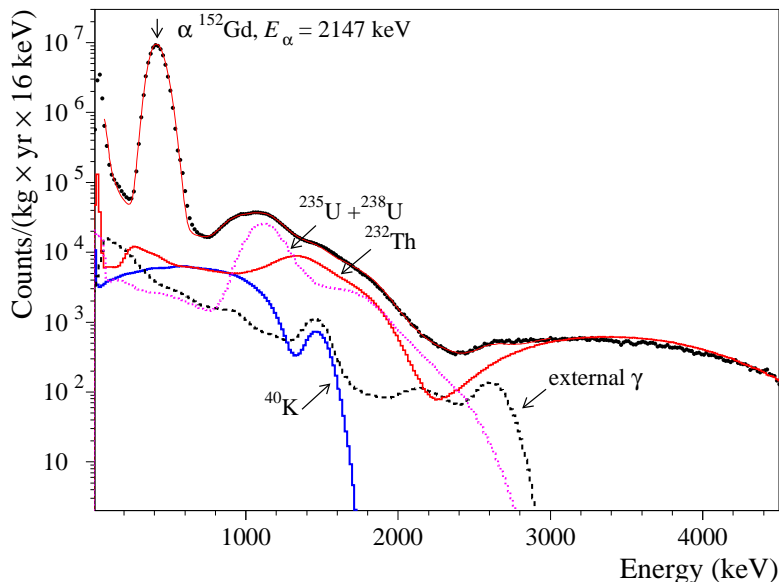


Figure 9: The background spectrum of the GSO detector for 0.969 yr kg of exposure (points) and the model of background (solid line) obtained by the fit of the data in the 60 – 3000 keV energy interval [44]. The most important internal ( $^{40}\text{K}$ , sum of  $^{235}\text{U}$  and  $^{238}\text{U}$ ,  $^{232}\text{Th}$ ) and external ( $\gamma$  radiation from the photomultiplier tube) components of background are shown. A peak at the energy  $\approx 420$  keV is due to the  $\alpha$  activity of  $^{152}\text{Gd}$ , while the background in the energy interval 0.8 – 2 MeV is caused mainly by  $\alpha$  decays of U/Th daughters.

### 3.2.5 Simulation of background energy spectra

To estimate possible contamination of a scintillator, especially by  $\beta$  active nuclides, one can fit an energy spectrum by Monte Carlo simulated models. As an example, the fit of the low background energy spectrum accumulated with GSO crystal scintillator in the experiment to search for  $2\beta$  decay of  $^{160}\text{Gd}$  [44] is presented in Fig. 9. The models of background were simulated with the help of the GEANT package [231, 232, 233]. For models presented in Fig. 9, an event generator DECAY0 [234] was used. This generator allows to take into account a number and types of emitted particles, their energies, directions of movement and times of emission. GEANT and EGS4 [235] packages are the most widely used to simulate background of scintillation detectors.

### 3.2.6 Low-temperature scintillating bolometers

An extremely high sensitivity to  $\alpha$  radioactive contamination of crystal scintillators can be reached by operation of a scintillator as low temperature scintillating bolometer thanks to a very high energy resolution and particle discrimination capability [51, 52, 53, 55]. The discrimination can be realized by analysis of heat and scintillation signals from a crystal scintillator (by using a different scintillation yield for ions [212], in particular for  $\alpha$  particles) or by only thermal pulse profile analysis [236].

The capability of low-temperature scintillating bolometers to screen  $\alpha$  radioactive contamination of crystal scintillators is illustrated in Fig. 10, where  $\alpha$  spectra gathered with two

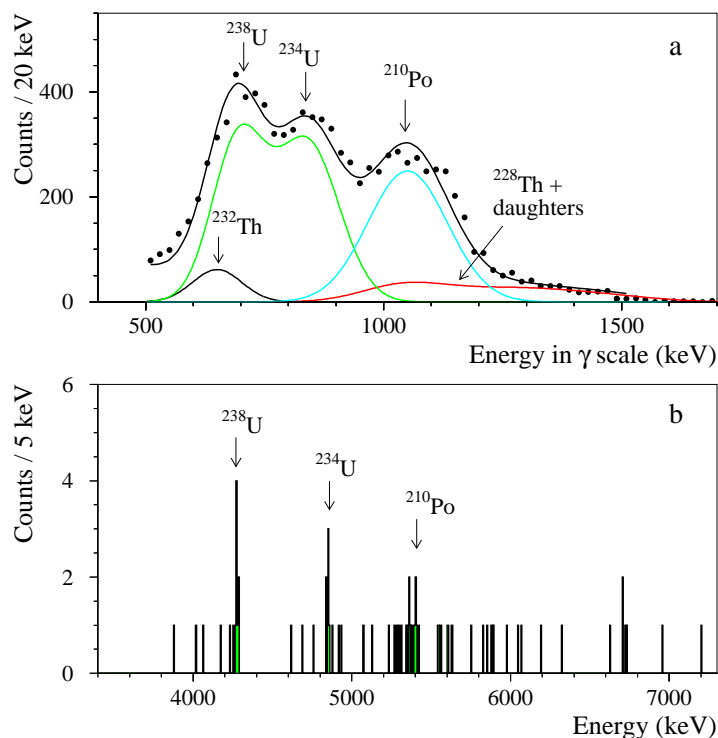


Figure 10: (a) Energy spectrum of  $\alpha$  events selected by pulse-shape discrimination from the data acquired by 589 g  $^{116}\text{CdWO}_4$  scintillation detector at the Gran Sasso underground laboratory over 1727 h together with the model which includes  $\alpha$  active nuclides of  $^{238}\text{U}$  and  $^{232}\text{Th}$  families [195]. (b) Energy spectrum of  $\alpha$  events measured by 34.5 g  $^{116}\text{CdWO}_4$  scintillating bolometer in a surface laboratory over 250 h [67]. An advantage of the high energy resolution and particle discrimination capability of the low-temperature scintillating bolometer is clearly visible.

samples of  $^{116}\text{CdWO}_4$  scintillator operated as a conventional scintillation detector and as a cryogenic scintillating bolometer are presented. A small sample of  $^{116}\text{CdWO}_4$  crystal (34.5 g) was measured over 250 h in a surface set-up [67]. The achieved sensitivity on the level of  $\sim 0.1$  mBq/kg for  $^{232}\text{Th}$ ,  $^{235}\text{U}$  and  $^{238}\text{U}$  (and their  $\alpha$  active daughters) competes with results of the long time measurements (1727 h) with much larger mass  $^{116}\text{CdWO}_4$  crystal scintillator (589 g) by using ultra-low background set-up deep underground at the Gran Sasso underground laboratory [195].

## 4 Data on radioactive contamination of scintillators

Data on radioactive contamination of different scintillators are presented in Tables 3-13. The main sources of radioactive contamination of scintillation materials are naturally occurring radionuclides of the  $^{232}\text{Th}$  and  $^{238}\text{U}$  families, and  $^{40}\text{K}$ . Activity of  $^{235}\text{U}$  with daughters is observed in some materials too. It should be stressed that the secular equilibrium of the U/Th chains is usually broken in scintillation materials. It means that the activities of  $^{238}\text{U}$ ,  $^{230}\text{Th}$ ,  $^{226}\text{Ra}$ ,  $^{210}\text{Pb}$  in the  $^{238}\text{U}$  family should be considered separately. The activity of  $^{210}\text{Po}$  should be also reported separately if a scintillation material was produced recently in comparison to the half-

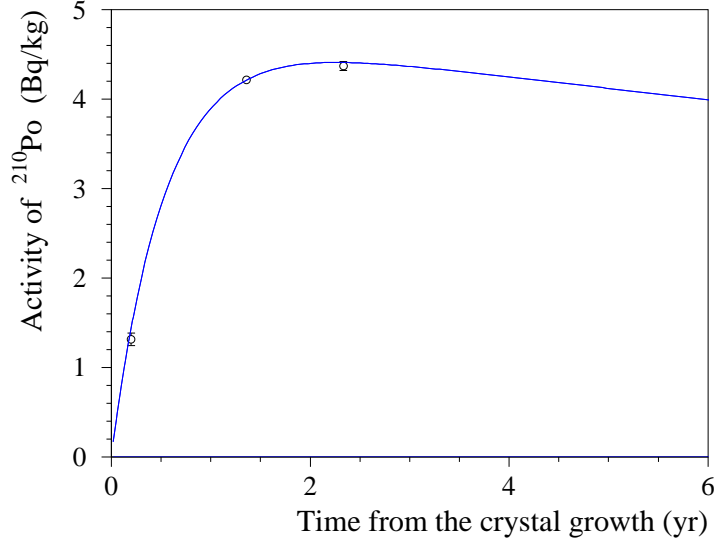


Figure 11: Time dependence of  $^{210}\text{Po}$  activity in  $\text{CaWO}_4$  crystal scintillator [196] (circles). The data is approximated by a function, describing the increase in  $^{210}\text{Po}$  due to the decay of  $^{210}\text{Pb}$  assuming essentially lower amount of  $^{210}\text{Po}$  after the crystal growth (solid line). The  $^{210}\text{Po}$  activity is beginning to decline after  $\sim 2.2$  yr due to decay of  $^{210}\text{Pb}$  ( $T_{1/2} = 22.2$  yr).

life of  $^{210}\text{Po}$  ( $T_{1/2} = 138.376(2)$  d). A time behaviour of  $^{210}\text{Po}$  activity in a  $\text{CaWO}_4$  crystal scintillator, in the case of essentially lower amount of  $^{210}\text{Po}$  after the crystal growth, is shown in Fig. 11. Similarly, contaminations by  $^{232}\text{Th}$ ,  $^{228}\text{Ra}$  and  $^{228}\text{Th}$  from the  $^{232}\text{Th}$  family, and activities of  $^{235}\text{U}$ ,  $^{231}\text{Pa}$  and  $^{227}\text{Ac}$  from the  $^{235}\text{U}$  family can be different. As an example of a strong disequilibrium of the  $^{232}\text{Th}$  chain we can refer the  $\text{CeF}_3$  crystal scintillator where the activity of  $^{232}\text{Th}$  exceeded the activity of  $^{228}\text{Th}$  by a factor 18 [205]. As for the  $^{238}\text{U}$  chain, its equilibrium is strongly broken e.g. in  $\text{CaWO}_4$  [155] where the activities of  $^{238}\text{U}$ ,  $^{226}\text{Ra}$  and  $^{210}\text{Po}$  relate as  $1 : 0.4 : 21$ . Both the  $^{232}\text{Th}$  and  $^{238}\text{U}$  chains were found strongly broken in  $\text{BaF}_2$  crystal scintillator, where radium accumulation ( $^{226}\text{Ra}$  from the  $^{238}\text{U}$  chain, and  $^{228}\text{Ra}$  from the  $^{232}\text{Th}$  chain) in the crystal was observed [244]. For this reason a reference date should be given for activities of relatively short living isotopes  $^{210}\text{Po}$ ,  $^{228}\text{Th}$ ,  $^{228}\text{Ac}$ .

Table 3: Radioactive contamination of organic scintillators.

Chain	Source	Activity (mBq/kg) in sample, Reference					
		Liquid scintillators			Plastic scintillators		
		Borexino, 278 t		KamLAND [238]	Polystyrene-based scintillator [239]	EJ-200 [240]	NE-102A [240]
	Phase I <sup>a</sup> [237]	Phase II [237]					
	<sup>14</sup> C	0.445(10)	0.445(10)	0.66(16)			
	<sup>39</sup> Ar			< 0.005			
	<sup>40</sup> K	< 1.1 × 10 <sup>-7</sup>	< 1.1 × 10 <sup>-7</sup>	3.4(3) × 10 <sup>-5</sup>		1.5(5)	2.2(7)
	<sup>85</sup> Kr	3.5(6) × 10 <sup>-6</sup>	< 6 × 10 <sup>-7</sup>	0.88(2)			
<sup>232</sup> Th	<sup>232</sup> Th	1.5(3) × 10 <sup>-8</sup>	< 4 × 10 <sup>-9</sup>	3.35(20) × 10 <sup>-7</sup>			
	<sup>228</sup> Ra					0.4(1)	9.2(4)
	<sup>228</sup> Th					0.5(1)	9.3(3)
	<sup>208</sup> Tl				< 0.00013 0.0015(4) mBq/m <sup>2</sup> <sup>b</sup>		
<sup>238</sup> U	<sup>238</sup> U	6.6(4) × 10 <sup>-8</sup>	< 10 <sup>-9</sup>	2.33(13) × 10 <sup>-8</sup>			
	<sup>226</sup> Ra					0.09(5)	0.96(13)
	<sup>210</sup> Pb			0.0584(11)			
	<sup>210</sup> Bi	2.3 × 10 <sup>-6</sup>	2.3(6) × 10 <sup>-6</sup>				
	<sup>210</sup> Po	8 × 10 <sup>-6</sup>	8 × 10 <sup>-6</sup>				

<sup>a</sup> The period before purification of liquid scintillator in 2010 – 2011 is called Phase I, the period after the purification is denoted as Phase II.

<sup>b</sup> Surface contamination.

Table 4: Radioactive contamination of fluorite crystal scintillators.

Chain	Source	Activity (mBq/kg) in sample, Reference						
		LiF(W)	CaF <sub>2</sub> (Eu)		SrF <sub>2</sub>	CeF <sub>3</sub>	BaF <sub>2</sub>	
		553 g [241]	370 g [159]	0.29 kg, 25 samples [206, 242]	53 g [243]	49 g [205]	734 g [42]	1.714 kg [244]
	<sup>40</sup> K	< 5.1	< 7			< 330		
	<sup>90</sup> Sr		< 4					
	<sup>137</sup> Cs	< 0.2	< 0.3					
	<sup>138</sup> La					< 60		
	<sup>147</sup> Sm		0.34(4)			< 80		
	<sup>176</sup> Lu					< 20		
	<sup>152</sup> Eu		10(2)					
<sup>232</sup> Th	<sup>232</sup> Th		0.05(1)			55(30)	400	< 4
	<sup>228</sup> Ra		< 0.6			890(270)		
	<sup>228</sup> Ac	< 1.6						
	<sup>228</sup> Th		0.13(2)			1010(10)		1.35(6) × 10 <sup>3</sup>
	<sup>224</sup> Ra				21(1)			
	<sup>220</sup> Rn			0.036(4) – 40.72(12)				
	<sup>208</sup> Tl	< 0.6						
<sup>235</sup> U	<sup>235</sup> U					< 40		< 0.6
	<sup>231</sup> Pa					< 50		< 0.7
	<sup>227</sup> Ac		0.011(7)	0.012(20) – 2.05(31)		< 20		< 70
<sup>238</sup> U	<sup>238</sup> U		0.06(1)			< 70		< 0.2
	<sup>234</sup> U					< 60		
	<sup>230</sup> Th					< 60		
	<sup>226</sup> Ra		1.3(2)		496(2)	< 60	1400	7.8(1) × 10 <sup>3</sup>
	<sup>214</sup> Pb	3.3(8)						
	<sup>214</sup> Bi	3.3(8)		0.052(23) – 75.3(4)				
	<sup>210</sup> Pb							0.99(1) × 10 <sup>3</sup>
	<sup>210</sup> Po		0.9(2)		72(6)	< 280		
Total α activity			8(2)			3400		

Table 5: Radioactive contamination of  $Y_3Al_5O_{12}:Nd$  [YAG(Nd)] and  $Li_6Eu(BO_3)_3$  crystal scintillators.

Chain	Source	Activity (mBq/kg) in sample, Reference		
		YAG(Nd)	$Li_6Eu(BO_3)_3$	
		7.16 g [227]	2.72 g [191]	6.15 g [160]
	$^{40}K$		< 1500	
	$^{60}Co$		< 26	
	$^{137}Cs$		< 81	
	$^{147}Sm$			454
	$^{207}Bi$		< 9	
	$^{152}Eu$		949(48)	
	$^{154}Eu$		212(35)	
$^{232}Th$	$^{232}Th$			3.5
	$^{228}Ac$		< 200	
	$^{212}Pb$		< 250	
	$^{208}Tl$		< 130	
$^{238}U$	$^{226}Ra$			2.9
	$^{214}Po$		< 170	
	$^{214}Bi$		< 70	
	$^{210}Po$			6.2
Total $\alpha$ activity		< 10		

Table 6: Radioactive contamination of ZnSe and Zn<sup>82</sup>Se crystal scintillators.

Chain	Source	Activity (mBq/kg) in sample, Reference		
		ZnSe 431 g [60]	Zn <sup>82</sup> Se ≈ 440 g, 3 samples [245]	Zn <sup>82</sup> Se 174 – 481 g, 26 samples [33]
<sup>232</sup> Th	<sup>232</sup> Th	0.0172(46)	< 0.005 – 0.013(4)	< 0.0005 – 0.009(1)
	<sup>228</sup> Th	0.0111(37)	0.022(4) – 0.032(7)	0.0023(8) – 0.027(2)
<sup>238</sup> U	<sup>238</sup> U	0.0246(55)	< 0.01 – 0.020(5)	< 0.001 – 0.013(2)
	<sup>234</sup> U	0.0178(33)		0.001(2) – 0.015(4)
	<sup>234</sup> U + <sup>226</sup> Ra	0.0178(33)	0.023(5) – 0.042(7)	
	<sup>230</sup> Th	0.0246(55)	0.017(4) – 0.019(5)	< 0.002 – 0.016(2)
	<sup>226</sup> Ra	0.0178(33)		0.004(1) – 0.018(2)
	<sup>218</sup> Po		0.020(5) – 0.024(5)	0.003(1) – 0.020(2)
	<sup>210</sup> Pb		0.100(12) – 0.250(17)	
	<sup>210</sup> Po	< 0.1		

Table 7: Radioactive contamination of NaI(Tl) crystal scintillators.

Chain	Source	Activity (mBq/kg) in sample, Reference							
		3.5 kg [224] UK DM	10.7 kg, [246, 247] 12.5 kg, [248, 249, 250] ANAIS	9.7 kg × 25 [209] DAMA/LIBRA	∅72 × 72 mm [251, 252] PICO-LON	3.4 – 9.6 kg [253, 254, 255] KIMS-NaI	8.47 kg [256] DM-Ice17	2 kg [257] SABRE	8 – 18 kg [258] COSINE-100
	<sup>3</sup> H		0.2	< 0.09					
	<sup>22</sup> Na			< 0.015					
	<sup>24</sup> Na			< 0.00026					
	<sup>40</sup> K		1.1 – 21	0.6	81(7)	0.8 – 1.5	17	0.3	0.5 – 2.5
	<sup>85</sup> Kr			< 0.01					
	<sup>87</sup> Rb			< 0.3				< 0.09	
	<sup>129</sup> I		0.94	0.95(6)			1		
<sup>232</sup> Th	<sup>232</sup> Th		0.0007 – 0.004	0.0085(5)	0.002 – 0.24		0.01	< 0.004	< 0.001 – 0.01
	<sup>228</sup> Ra						0.16		
	<sup>228</sup> Th	0.014		0.002 – 0.03		0.0008 – 0.04	0.17 – 0.18		
	<sup>216</sup> Po		0.02		0.013(8)				
<sup>238</sup> U	<sup>238</sup> U	< 0.005		0.0044(7)	< 0.0005 – 0.52		0.017	< 0.01	< 0.0002 – < 0.0015
	<sup>234</sup> U		2.7 – 10	0.0158(16)			0.14		
	<sup>226</sup> Ra	0.045	0.2	0.0217(11)	0.105(17)	< 0.0002 – < 0.015	0.93 – 0.96		
	<sup>210</sup> Pb		0.7 – 3.15	0.0242(16)	0.03 – 9.6		1.5		
	<sup>210</sup> Po		0.6						
Total α activity			0.58 – 3.15	≈ 0.08		0.48 – 3.29			0.74 – 3.20

Table 8: Radioactive contamination of CsI(Tl) and CsI(Na) crystal scintillators.

Chain	Source	Activity (mBq/kg) in sample, Reference			
		CsI(Tl)			CsI(Na)
		2 kg $\times$ 93 [208] TEXONO	6.6 kg [187] KIMS	4.55 kg, 3 samples [259] China Dark matter Experiment	$\approx$ 2 kg [260]
	$^{40}\text{K}$				17(16)
	$^{87}\text{Rb}$		1.2(4)		61
	$^{134}\text{Cs}$		6.3(7)		26(2)
	$^{137}\text{Cs}$	61(2)	14.1(11)	72.9(1) – 86.6(1)	28(3)
$^{232}\text{Th}$	$^{232}\text{Th}$	0.0091(2)	0.0015(3)		$< 4$
	$^{228}\text{Th}$			0.017(2) – 0.069(3)	
$^{235}\text{U}$	$^{235}\text{U}$	$< 0.0016$			
	$^{227}\text{Ac}$			$< (0.2 - 1.1) \times 10^{-3}$	
$^{238}\text{U}$	$^{238}\text{U}$	0.0101(2)	0.009(3)		$< 12$
	$^{226}\text{Ra}$			0.022(2) – 0.087(3)	

Table 9: Radioactive contamination of LiI(Eu), SrI<sub>2</sub>(Eu), LaCl<sub>3</sub>(Ce), CeBr<sub>3</sub>, Cs<sub>2</sub>HfCl<sub>6</sub> and YVO<sub>4</sub> crystal scintillators.

Chain	Source	Activity (mBq/kg) in sample, Reference					
		LiI(Eu)	SrI <sub>2</sub> (Eu)	LaCl <sub>3</sub> (Ce)	CeBr <sub>3</sub>	Cs <sub>2</sub> HfCl <sub>6</sub>	YVO <sub>4</sub>
		26 g 2 samples [198]	∅13 × 11 mm 6.6 g [197]	49.7 g [261]	222 g [262]	12 g [189]	22 g [150]
	<sup>40</sup> K	< 177	< 200		< 1.9	< 0.18	< 220
	<sup>60</sup> Co				1.4(4)	< 19	< 2.2
	<sup>82</sup> Br				18(4)		
	<sup>90</sup> Sr- <sup>90</sup> Y	< 160	< 90				
	<sup>132</sup> Cs					25(8)	
	<sup>134</sup> Cs					52(6)	
	<sup>137</sup> Cs	< 22	53(11)		< 0.9	830(90)	< 8.6
	<sup>138</sup> La		< 20	4.12(8) × 10 <sup>5</sup>	7.4(10)		
	<sup>139</sup> Ce				4.3(3)		
	<sup>147</sup> Sm						2.3(5)
	<sup>152</sup> Eu	< 47	< 108				
	<sup>154</sup> Eu	< 42	< 67				
	<sup>176</sup> Lu		< 143				
	<sup>181</sup> Hf					14.0(7)	14.0(7)
<sup>232</sup> Th	<sup>232</sup> Th		< 3				8(1)
	<sup>228</sup> Ac	< 88	< 68				
	<sup>228</sup> Ra				< 0.7	< 12	< 12
	<sup>228</sup> Th	< 0.4	6(2)	< 0.36	< 2.0	< 6.3	< 10
<sup>235</sup> U	<sup>235</sup> U			1.5(4) × 10 <sup>3</sup>	< 1.5	< 26	
	<sup>227</sup> Ac				300(20)		
<sup>238</sup> U	<sup>238</sup> U		< 40		< 135		1373(2)
	<sup>234</sup> Th					< 8.6	1600(400)
	<sup>234m</sup> Pa					< 3.7	1200(500)
	<sup>226</sup> Ra	< 1.1	100(14)	< 35	< 0.5		5(1)
	<sup>210</sup> Pb	< 480	< 180		< 600		
	<sup>210</sup> Po	< 2	< 60				5(1)

Table 10: Radioactive contamination of  $\text{Gd}_2\text{SiO}_5$  (GSO) and  $\text{Bi}_4\text{Ge}_3\text{O}_{12}$  (BGO) crystal scintillators.

Chain	Source	Activity (mBq/kg) in sample, Reference				
		GSO		BGO		
		635 g [44]	1.744 kg [204]	0.28 – 0.49 kg [185]	46 g [157]	Table 1 in [263]
	$^{40}\text{K}$	< 14				< 7
	$^{138}\text{La}$	< 55				
	$^{147}\text{Sm}$		$\approx 100$			
	$^{207}\text{Bi}$			520 – 930	3000	7(2) – 4400
$^{232}\text{Th}$	$^{232}\text{Th}$	< 6.5		< 1.1		
	$^{228}\text{Ra}$	< 9	733			
	$^{228}\text{Th}$	2.287(13)	107			
	$^{212}\text{Pb}$					6(4)
	$^{208}\text{Tl}$					3(2)
$^{235}\text{U}$	$^{227}\text{Ac}$	0.948(9)				
	$^{231}\text{Pa}$	< 0.08				
$^{238}\text{U}$	$^{238}\text{U}$	< 2	< 2	< 0.3		
	$^{230}\text{Th}$	< 9				
	$^{226}\text{Ra}$	0.271(4)	< 2			
	$^{210}\text{Pb}$		198			
	$^{210}\text{Po}$	< 0.8				
Total $\alpha$ activity		40	217			

Table 11: Radioactive contamination of molybdate crystal scintillators.

Chain	Source	Activity (mBq/kg) in sample, Reference						
		$\text{Li}_2\text{MoO}_4$	$\text{Li}_2^{100}\text{MoO}_4$	$\text{Li}_2\text{Mg}_2(\text{MoO}_4)_3$	$\text{ZnMoO}_4$	$\text{Zn}^{100}\text{MoO}_4$	$\text{CaMoO}_4$	$^{48\text{depl}}\text{Ca}^{100}\text{MoO}_4$
		151 – 242 g, [35]	186 – 204 g, [35]	10.2 g, [71]	$\approx 340$ g, [35]	$\approx 380$ g, [35]	82 – 100 g, [229]	$\approx 310$ g, [76]
	$^{40}\text{K}$	< 3.2 – 62(2)	< 3.5				< 1.1	
	$^{90}\text{Sr}$						< 23	
	$^{190}\text{Pt}$	< 0.018	< 0.003		0.0026(13)			
$^{232}\text{Th}$	$^{232}\text{Th}$	< 0.018	< 0.003	< 0.95	< 0.0014	< 0.008	< 0.7	< 0.05
	$^{228}\text{Th}$	< 0.018	< 0.006	< 1.1	< 0.005	< 0.008	0.04(2) – 0.42(17)	
$^{238}\text{U}$	$^{238}\text{U}$	< 0.018	< 0.005	< 0.95	< 0.003	0.010(4) – 0.039(7)	< 0.5	0.98
	$^{234}\text{U}$	< 0.018	< 0.007	< 1.7	< 0.003	0.011(6) – 0.043(10)		
	$^{230}\text{Th}$	< 0.018	< 0.003		< 0.0014	< 0.017		
	$^{226}\text{Ra}$	< 0.037 – 0.130(19)	< 0.007	< 1.7	< 0.006	0.014(3) – 0.023(4)	0.13(4) – 2.5(5)	0.065
	$^{210}\text{Pb}$						< 17	7.3
	$^{210}\text{Po}$	0.08(3) – 0.20(4)	0.06(1) – 0.23(2)	5.6(13)	0.575(18) – 1.320(30)	0.81(3) – 2.39(5)	< 8 – 550(20)	
$^{235}\text{U}$	$^{235}\text{U}$	< 0.018	< 0.005	< 1.9	< 0.003	< 13		
	$^{231}\text{Pa}$	< 0.018	< 0.003		< 0.0014	< 0.008		
	$^{227}\text{Th}$	< 0.018	< 0.005		< 0.003	< 0.009		
	$^{223}\text{Ra}$			< 1.1				
	$^{211}\text{Bi}$							0.47

Table 12: Radioactive contamination of cadmium tungstate ( $\text{CdWO}_4$ ) crystal scintillators.

Chain	Source	Activity (mBq/kg) in sample, Reference						
		$\text{CdWO}_4$				$^{106}\text{CdWO}_4$	$^{116}\text{CdWO}_4$	
		72 g [264]	1046 g [201, 265]	434 g [147]	496 g [65]	215 g [266, 39]	330 g [45, 153]	580 g, 582 g [267, 67, 41]
	$^{40}\text{K}$	3.6(20)	< 1.7	< 5		< 1.4	0.3(1)	< 0.2
	$^{90}\text{Sr}$	< 1.4	< 3				< 0.2	
	$^{90}\text{Sr}-^{90}\text{Y}$			< 1		< 0.3		
	$^{110m}\text{Ag}$							0.12(4)
	$^{113}\text{Cd}$	580	580(20)	558(4)		182	91(5)	100(10)
	$^{113m}\text{Cd}$	30(10)	150(10)	< 3.4		$116(4) \times 10^3$	1.1(1)	460(20)
	$^{137}\text{Cs}$	< 0.9	< 0.3	< 0.3			0.43(6)	
	$^{147}\text{Sm}$			< 0.01				
	$^{180}\text{W}$						0.018(7)	
	$^{190}\text{Pt}$	< 0.1					< 0.001	
$^{232}\text{Th}$	$^{232}\text{Th}$			< 0.026	< 0.004	< 0.07	0.053(9)	< 0.08
	$^{228}\text{Ra}$						< 0.004	
	$^{228}\text{Th}$	0.015(8)	< 0.003	0.008(4)		0.042(4)	0.039(2)	0.02 – 0.067(4) <sup>a</sup>
$^{235}\text{U}$	$^{235}\text{U}$							< 0.13
$^{235}\text{U}$	$^{227}\text{Ac}$	< 0.005	< 0.005				0.0014(9)	< 0.002
$^{238}\text{U}$	$^{238}\text{U}$		< 1.3		0.038	< 0.6	< 0.6	0.3(1) – 0.5(2)
	$^{234m}\text{Pa}$						< 0.2	
	$^{234}\text{U}$				0.013			
	$^{230}\text{Th}$					< 0.4	< 0.5	< 0.05
	$^{226}\text{Ra}$	< 0.04	< 0.007	< 0.018		0.012(3)	< 0.004	< 0.005
	$^{210}\text{Pb}$						< 0.4	
	$^{210}\text{Po}$			< 0.063		< 0.2		0.23(8)
	Total $\alpha$ activity			0.26(4)		2.1(2)	1.40(10)	2.10(2) – 2.93(2)

<sup>a</sup>The range of  $^{228}\text{Th}$  activity is due to the decay of  $^{228}\text{Th}$  during the long time measurements.

Table 13: Radioactive contamination of magnesium ( $\text{MgWO}_4$ ), calcium ( $\text{CaWO}_4$ ), zinc ( $\text{ZnWO}_4$ ) and lead ( $\text{PbWO}_4$ ) tungstate crystal scintillators.

Chain	Source	Activity (mBq/kg) in sample, Reference								
		MgWO <sub>4</sub>	CaWO <sub>4</sub>				ZnWO <sub>4</sub>		PbWO <sub>4</sub>	
		0.9 g [216]	54 g [268]	189 g [155]	328 – 740 g [196]	155 – 310 g [269, 270]	163 g [192]	117 – 699 g [156]	182 g [271]	454 g <sup>b</sup> [161]
	<sup>40</sup> K	< 1.6 × 10 <sup>3</sup>	< 100	< 12	< 21	< 20	< 321	< 0.02		
	<sup>65</sup> Zn							0.5(1) – 0.8(2)		
	<sup>90</sup> Sr– <sup>90</sup> Y	< 1.5 × 10 <sup>3</sup>		< 70	< 26			< 0.1		
	<sup>137</sup> Cs		< 10	< 0.8		< 1.2		< 0.05		
	<sup>147</sup> Sm	< 540	6(2)	0.49(4)				< 0.01		0.007(5)
<sup>232</sup> Th	<sup>232</sup> Th	< 280	< 0.2	0.69(10)	< 9	0.009(2)		< 0.03		0.051(8)
	<sup>228</sup> Ra					< 2.1, 0.015(4)		< 0.02		
	<sup>228</sup> Ac		< 40				< 125			
	<sup>228</sup> Th	< 50	< 30	0.6(2)	< 6	< 1.6		0.002(2) – 0.018(2)	< 13	
	<sup>212</sup> Pb		< 200				< 316			
	<sup>212</sup> Bi		< 80				< 267			
<sup>235</sup> U	<sup>235</sup> U					0.040(4)	< 3610			
	<sup>227</sup> Ac			1.6(3)		0.098(20)		< 0.003 – 0.011(3)		
	<sup>211</sup> Pb						< 162			
<sup>238</sup> U	<sup>238</sup> U		40(4)	14.0(5)	38(14) – 330(17)	< 68, 1.01(2)				< 0.01
	<sup>238</sup> U+ <sup>234</sup> U							< 0.08		
	<sup>234m</sup> Pa		< 400				< 560			
	<sup>234</sup> U					1.08(3)				< 0.007
	<sup>230</sup> Th					0.056(5)		< 0.07		0.178(15)
	<sup>226</sup> Ra	< 50	7(2)	5.6(5)	4(2) – 107(11)	< 2.2 – 58, 0.04(1)	< 30 × 10 <sup>3</sup>	0.002(1) – 0.025(6)	< 10	1.403(43)
	<sup>214</sup> Pb		< 100				< 115			
	<sup>214</sup> Bi		< 80			0.047(5)	< 159			
	<sup>210</sup> Pb	< 2.4 × 10 <sup>3</sup>	900(70)	< 430	< 190 – 4800(200)				(53 – 79) × 10 <sup>3</sup>	
	<sup>210</sup> Po	5.7(4) × 10 <sup>3</sup>	780(20)	291(5)	26(9) – 1316(17)	0.018(4)		< 0.01		186(1)
Total α activity			930 <sup>a</sup>	400	240(20) – 1400(30)	1.2 – 107, 3.08(4)		0.18(3) – 2.3(2)		

<sup>a</sup> Estimated from the spectra presented in Fig. 13 of Ref. [268].

<sup>b</sup> PbWO<sub>4</sub> crystal produced from archaeological lead.

Radioactive contamination of scintillators is summarized in Table 14 where the data for germanium crystals used in ultra-low background HP Ge detector [272, 273] are given for comparison. As one can see in Tables 3-13, authors present their data for different members of the  $^{232}\text{Th}$  and  $^{238}\text{U}$  families. In most cases the measured nuclides are short living daughters of  $^{226}\text{Ra}$  and  $^{228}\text{Th}$ . Therefore, in Table 10 we present data for  $^{228}\text{Th}$  and  $^{226}\text{Ra}$ . Activity of  $^{210}\text{Po}$  is typically measured in scintillators, while its origin is mostly contamination by lead ( $^{210}\text{Pb}$ ). For this reason data on  $^{210}\text{Pb}$  activity is presented in Table 14. However, one should keep in mind that equilibrium between  $^{210}\text{Pb}$  and its daughter  $^{210}\text{Po}$  is broken as usual, as it was discussed above.

Table 14: Radioactive contamination of scintillators (mBq/kg). Data for germanium crystals of HP Ge detectors [272, 273] are given for comparison.

Scintillator	$^{40}\text{K}$	$^{228}\text{Th}$	$^{226}\text{Ra}$	$^{210}\text{Pb}$	Total $\alpha$ (U + Th)	Particular radioactivity
Plastic scintillator	2	$< 0.0001 - 9$	$0.09 - 1$			$^{14}\text{C}$
Liquid scintillator	$< 1 \times 10^{-7} - 3 \times 10^{-5}$	$(< 4 \times 10^{-9} - 3 \times 10^{-7})^a$	$(< 10^{-9} - 6 \times 10^{-8})^b$	$2 \times 10^{-6} - 0.06$		$^{14}\text{C}$
LiF(W)	$< 5$	$< 0.6$	3			$^{180}\text{W}$
CaF <sub>2</sub> (Eu)	$< 7$	0.13 – 41	0.05 – 75	0.9	8	$^{48}\text{Ca}$ , $^{151}\text{Eu}$
SrF <sub>2</sub>		21	496	$72^c$		
CeF <sub>3</sub>	$< 330$	1010	$< 60$	$< 280^c$		
BaF <sub>2</sub>		$1.4 \times 10^3$	$(1.4 - 7.8) \times 10^3$	990		
YAG(Nd)					$< 20$	$^{144}\text{Nd}$ , $^{150}\text{Nd}$
Li <sub>6</sub> Eu(BO <sub>3</sub> ) <sub>3</sub>	$< 1500$	$3.5^a$	2.9	6.2		$^{151}\text{Eu}$ , $^{152}\text{Eu}$ , $^{154}\text{Eu}$
ZnSe		$< 0.0004 - 0.02^a$	$< 0.0004 - 0.03^b$	$< 0.1^c$		$^{65}\text{Zn}$ , $^{75}\text{Se}$ , $^{82}\text{Se}$
Zn <sup>82</sup> Se		0.02 – 0.03	$0.02 - 0.04^d$	0.1 – 0.3		$^{82}\text{Se}$
LaCl <sub>3</sub> (Ce)		$< 0.4$	$< 40$			$^{138}\text{La}$ , $^{235}\text{U}$
Cs <sub>2</sub> HfCl <sub>6</sub>	$< 0.18$	$< 6$				$^{174}\text{Hf}$
LiI(Eu)	$< 180$	$< 0.4$	$< 1.1$	$< 2^c$		$^{151}\text{Eu}$
NaI(Tl)	0.3 – 81	0.0008 – 0.18	$< 0.0002 - 1$	0.02 – 10	0.08 – 3	$^3\text{H}$ , $^{129}\text{I}$
SrI <sub>2</sub> (Eu)	$< 200$	6	100	$< 180$		$^{151}\text{Eu}$
CsI(Na)	17	$< 0.4^a$	$< 12^b$			$^{134}\text{Cs}$ , $^{137}\text{Cs}$
CsI(Tl)		$(0.009^a - 0.07)$	$(0.009^b - 0.09)$			$^{134}\text{Cs}$ , $^{137}\text{Cs}$
CeBr <sub>3</sub>	$< 1.9$	$< 2$	$< 0.5$	$< 600$		$^{82}\text{Br}$ , $^{139}\text{Ce}$
GSO(Ce)	$< 14$	2.3 – 107	0.27	200	40 – 220	$^{152}\text{Gd}$
BGO	$< 7$	6				$^{209}\text{Bi}$ , $^{207}\text{Bi}$
Li <sub>2</sub> MoO <sub>4</sub>	$< 3 - 60$	$< 0.018$	$< 0.04 - 0.13$	$(0.08 - 0.2)^c$		$^{100}\text{Mo}$
Li <sub>2</sub> <sup>100</sup> MoO <sub>4</sub>	$< 3$	$< 0.006$	$< 0.007$	$(0.06 - 0.23)^c$		$^{100}\text{Mo}$
Li <sub>2</sub> Mg <sub>2</sub> (MoO <sub>4</sub> ) <sub>3</sub>		$< 1.1$	$< 1.7$	$6^c$		$^{100}\text{Mo}$
ZnMoO <sub>4</sub>		$< 0.005$	$< 0.006$	$0.6-1.3^c$		$^{100}\text{Mo}$
Zn <sup>100</sup> MoO <sub>4</sub>		$< 0.008$	0.014 – 0.023	$0.8 - 2.4^c$		$^{100}\text{Mo}$
CaMoO <sub>4</sub>	$< 1.1$	0.04 – 0.4	0.13 – 2.5	$< 8 - 550^c$		$^{48}\text{Ca}$ , $^{100}\text{Mo}$
<sup>48depl</sup> Ca <sup>100</sup> MoO <sub>4</sub>		$< 0.05^a$	0.07	7		$^{48}\text{Ca}$ , $^{100}\text{Mo}$
MgWO <sub>4</sub>	$< 1.6 \times 10^3$	$< 50$	$< 50$	$5.7 \times 10^3^c$	$5.7 \times 10^3$	$^{180}\text{W}$
CaWO <sub>4</sub>	$< 12$	0.6	0.04 – 107	$< 190 - 4800$	1 – 1400	$^{48}\text{Ca}$ , $^{180}\text{W}$
ZnWO <sub>4</sub>	$< 0.02$	0.002 – 0.018	0.002 – 0.025	$< 0.01^c$	0.18 – 2.3	$^{65}\text{Zn}$ , $^{180}\text{W}$
CdWO <sub>4</sub>	$< 1.7 - 4$	$< 0.003 - 0.015$	$< 0.007$	$< 0.06^c$	0.26	$^{113}\text{Cd}$ , $^{116}\text{Cd}$ , $^{180}\text{W}$
<sup>106</sup> CdWO <sub>4</sub>	$< 1.4$	0.042	0.012	$< 0.2^c$	2.1	$^{113m}\text{Cd}$ , $^{113}\text{Cd}$ , $^{116}\text{Cd}$ , $^{180}\text{W}$
<sup>116</sup> CdWO <sub>4</sub>	$< 0.2 - 0.3$	0.02 – 0.07	$< 0.004$	$0.23^c$	1.4 – 2.9	$^{113m}\text{Cd}$ , $^{113}\text{Cd}$ , $^{116}\text{Cd}$ , $^{180}\text{W}$
PbWO <sub>4</sub>		$< 13$	$< 10$	$(5 - 8) \times 10^{4c}$		$^{210}\text{Pb}$ , $^{180}\text{W}$
PbWO <sub>4</sub> <sup>2</sup>		0.05 <sup>a</sup>	1.4	$190^c$		$^{210}\text{Pb}$ , $^{180}\text{W}$
HP Ge		$< 2 \times 10^{-5a}$	$< 2 \times 10^{-5b}$			$^{76}\text{Ge}$

<sup>a</sup> Activity of  $^{232}\text{Th}$ .

<sup>b</sup> Activity of  $^{238}\text{U}$ .

<sup>c</sup> Activity of  $^{210}\text{Po}$ .

<sup>d</sup> Activity of  $^{238}\text{U} + ^{226}\text{Ra}$ .

<sup>e</sup> Produced from ancient lead.

Liquid scintillators are the most radiopure scintillation materials with a nBq/kg – pBq/kg radiopurity level of  $^{40}\text{K}$ , U and Th [237, 238]. However, cosmogenic  $^{14}\text{C}$  remains the main source of the background counting rate (0.4 – 0.7 mBq/kg, at energies below 0.25 MeV) of large low-background liquid scintillation detectors, despite the significant efforts to reduce its concentration. Radioactive contamination of plastic scintillators is significantly higher. It can be explained by polymerization process and mechanical treatment of the material, as well as by absence of a strong motivation to obtain highly radiopure scintillation material similar to the Borexino and KamLAND experiments. Crystal scintillators like  $\text{ZnWO}_4$ ,  $\text{CdWO}_4$  (including produced from enriched  $^{106}\text{Cd}$  and  $^{116}\text{Cd}$ ),  $\text{Li}_2\text{MoO}_4$ ,  $\text{ZnMoO}_4$  (including enriched in  $^{100}\text{Mo}$ ),  $\text{ZnSe}$  (including enriched in  $^{82}\text{Se}$ ), specially developed for low background experiments  $\text{CaF}_2(\text{Eu})$ ,  $\text{NaI}(\text{Tl})$ ,  $\text{CsI}(\text{Tl})$  and  $\text{CaMoO}_4$  have rather low contamination by  $^{226}\text{Ra}$  and  $^{228}\text{Th}$  on the level of  $\sim 0.001 - 0.1$  mBq/kg.

A level of crystal scintillators radiopurity is determined first of all by their chemical composition. For instance,  $\text{CdWO}_4$  and  $\text{ZnWO}_4$  crystals always show low level of internal activity, while  $\text{CaWO}_4$  has much higher level of radioactive contamination. Fig. 12 demonstrates the large difference in radiopurity of  $\text{CaWO}_4$ ,  $\text{CdWO}_4$  and  $\text{PbWO}_4$ . Scintillators containing rare earth elements (GSO,  $\text{CeF}_3$ ) have much higher level of radioactive trace pollution too. It is due to source of rare earth mining: they usually are extracted from monazites – minerals containing a few percents of uranium and thorium. Energy spectra of  $\text{CaF}_2(\text{Eu})$  and  $\text{CeF}_3$  crystal scintillators measured in the same conditions of the DAMA R&D low background set-up in the Gran Sasso underground laboratory of I.N.F.N. (Italy) are presented in Fig. 13. The background counting rate of the  $\text{CeF}_3$  detector is two orders of magnitude higher due to the higher contamination by thorium and uranium. Rather high radioactive contamination of  $\text{BaF}_2$  by radium ( $^{226}\text{Ra}$  and  $^{228}\text{Ra}$ ) can be explained by similar chemical properties of barium and radium. It should be stressed that the chemical and physical processes involved in scintillators production are sensitive to the chemical properties of materials. Therefore, it might be more accurate to discuss contamination of materials by chemical elements, not by certain isotopes.

Presence of radioactive elements (see Table 2) obviously determines radioactivity of scintillators like  $\beta$  active  $^{113}\text{Cd}$  in  $\text{CdWO}_4$ ,  $\alpha$  active  $^{152}\text{Gd}$  in GSO,  $^{138}\text{La}$  in  $\text{LaCl}_3$  and  $\text{LaBr}_3$ ,  $^{176}\text{Lu}$  in  $\text{Lu}_2\text{SiO}_5$  and  $\text{LuI}_3$ . Beta active  $^{210}\text{Pb}$  is usually present in  $\text{PbWO}_4$  and  $\text{PbMoO}_4$  (however, this problem can be overcome by producing lead containing scintillators from archaeological lead [51, 216, 161]).

Two neutrino  $2\beta$  decay, despite it is the rarest decay ever observed, becomes one of the most significant background sources in the experiments aiming to search for  $0\nu 2\beta$  decay with smaller  $Q_{2\beta}$ . For this reason the AMoRE collaboration developed  $\text{CaMoO}_4$  crystal scintillators enriched in the isotope  $^{100}\text{Mo}$  and depleted in  $^{48}\text{Ca}$  [274, 56]. Another example is  $\text{CdMoO}_4$  crystal scintillators proposed to search for  $0\nu 2\beta$  decay of  $^{116}\text{Cd}$  and  $^{100}\text{Mo}$  [275]: in this case the  $2\nu 2\beta^-$  decays of  $^{100}\text{Mo}$  will generate background in the region of interest of  $^{116}\text{Cd}$ .

## 5 Development of radiopure scintillation materials

A strong R&D is required to obtain a radiopure scintillation material. There were several systematic programmes to elaborate radiopure scintillators. Extremely radiopure liquid scintillators were developed for the Borexino [276] and KamLAND [277] neutrino experiments. Two factors which determine success of the projects are as following: 1) organic materials in

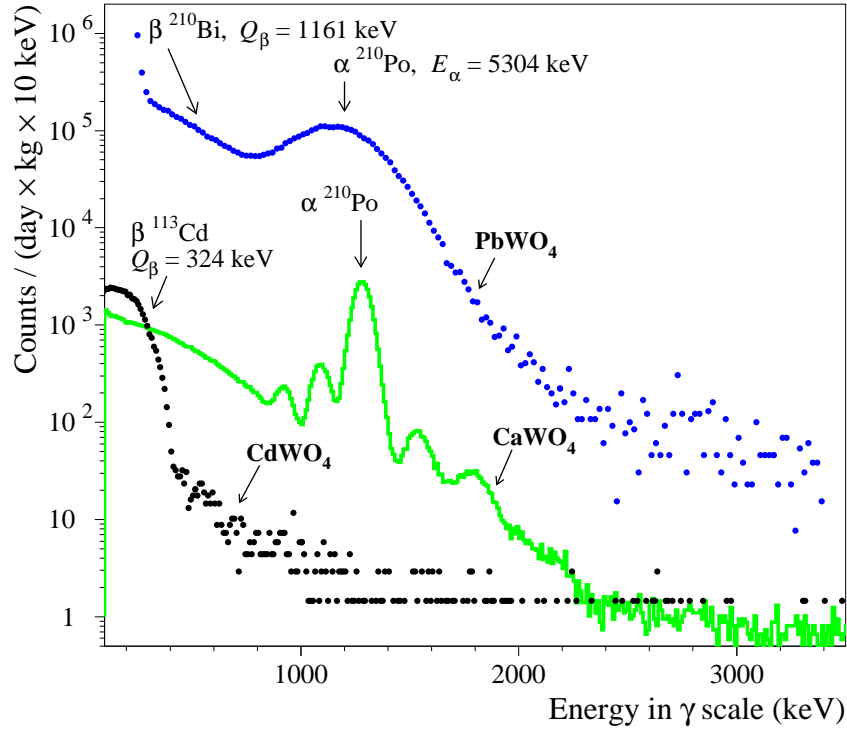


Figure 12: Energy spectra of  $\text{CaWO}_4$  (189 g, 1734 h),  $\text{CdWO}_4$  (448 g, 37 h), and  $\text{PbWO}_4$  (185 g, 2.15 h) scintillation crystals measured in the low background set-up in the Solotvina Underground Laboratory (the  $\text{PbWO}_4$  crystal was measured without shield). The  $\text{CaWO}_4$  crystal is considerably polluted by radionuclides from U and Th chains [230]. Beta decay of  $^{113}\text{Cd}$  ( $T_{1/2} = 8.04 \times 10^{15}$  years) dominates in the low energy part of the  $\text{CdWO}_4$  spectrum [146, 147].  $\text{PbWO}_4$  crystal is contaminated by  $^{210}\text{Pb}$  [271].

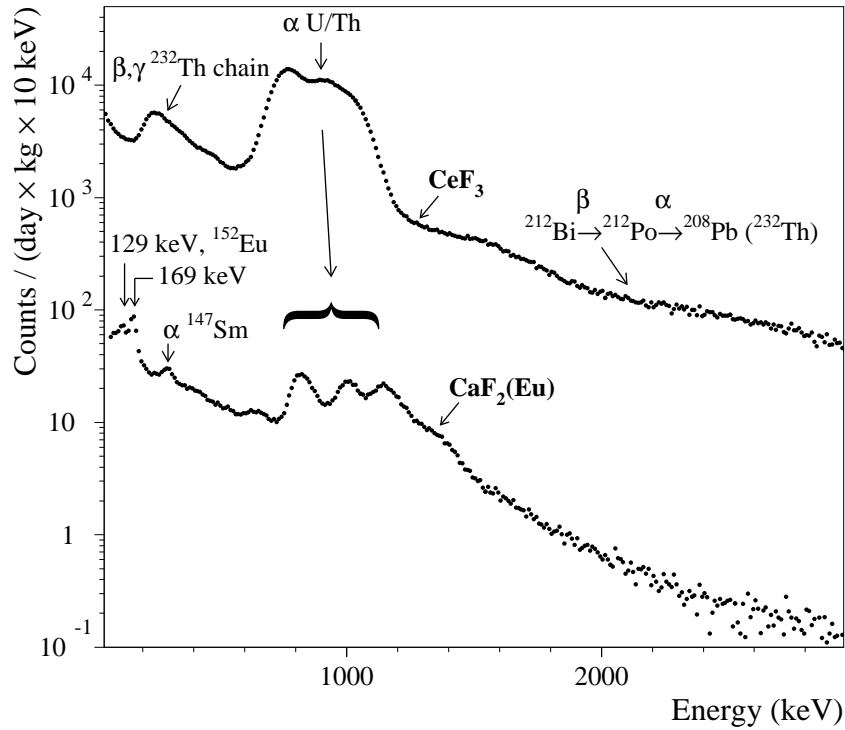


Figure 13: Energy spectra of  $\text{CeF}_3$  (49 g, 2142 h) and  $\text{CaF}_2(\text{Eu})$  (370 g, 7426 h) scintillation crystals measured in the DAMA R&D low background set-up in the Gran Sasso underground laboratory of I.N.F.N. (Italy). The  $\text{CeF}_3$  crystal is considerably polluted by radionuclides from Th and U chains on the  $\sim \text{Bq/kg}$  level (see for details [205]). The background of the  $\text{CaF}_2(\text{Eu})$  detector is two orders of magnitude lower, and caused by  $\alpha$  activity of U/Th daughters on the level of a few mBq/kg [159]. In the low energy part of the spectrum accumulated with the  $\text{CaF}_2(\text{Eu})$  crystal one can see peaks from cosmogenic (or / and neutron induced)  $^{152}\text{Eu}$  ( $\approx 10 \text{ mBq/kg}$ ), as well as  $\alpha$  peak of  $^{147}\text{Sm}$  presented in the crystal with an activity of  $\approx 0.3 \text{ mBq/kg}$ .

principle are much less contaminated in comparison to inorganic materials; 2) liquids can be effectively purified by distillation, nitrogen purging, water extraction and/or column purification [276, 278].

Very low background NaI(Tl) scintillators have been produced by Saint-Gobain for the DAMA/LIBRA dark matter experiment [209, 279, 280]; several R&D are in progress to develop radiopure NaI(Tl) scintillators [248, 252, 253, 256, 257]. Low background CsI(Tl) were developed in the framework of the KIMS dark matter experiment [187, 208]. Dependence of radiopurity of CsI(Tl) on crystal growth conditions was studied in [208]. Authors reported a clear increase of  $^{226}\text{Ra}$  and  $^{228}\text{Th}$  activity along the crystals during the crystal growth process due to increase of the melt contamination. Clear increase of radioactive contamination along the crystal boule was observed in  $^{116}\text{CdWO}_4$  crystal [281].

Achievement of a high radiopurity level of scintillators needs a variety of special measures as it was demonstrated by development of radiopure crystal scintillators for double beta decay experiments:  $^{106}\text{CdWO}_4$  [266],  $^{116}\text{CdWO}_4$  [195],  $^{48\text{depl}}\text{Ca}^{100}\text{MoO}_4$  [37, 282],  $\text{Zn}^{82}\text{Se}$  [283],  $\text{Zn}^{100}\text{MoO}_4$  [284, 285, 286, 287, 35] and  $\text{Li}_2^{100}\text{MoO}_4$  [62, 288, 35].

A programme to develop radiopure scintillation materials for experiments to search for rare processes could comprise the following steps [289]:

1. Careful selection and deep purification of raw materials is supposed to be the most important issue that needs addressing. Purification of metals (Zn, Cd, Pb, Bi) by vacuum distillation, zone melting, and filtering are very promising approaches [290, 291, 292], while further study is necessary for the purification of Li, Na, Ca, Se, Cs, Ba, Ce, Gd, W, Tl. Molybdenum can be deeply purified by combination of a double sublimation of molybdenum oxide with subsequent recrystallization in aqueous solutions [285].

2. Two step re-crystallization, involving inspection and assessment of the produced scintillators after each step. A promising result was obtained with the  $^{116}\text{CdWO}_4$  crystal scintillator by re-crystallization. The radioactive contamination of a sample of  $^{116}\text{CdWO}_4$  scintillator by thorium was reduced by one order of magnitude after the second crystallization procedure [281]. A larger number of recrystallization steps is limited by evaporation of components of melt (e.g. dominant evaporation of cadmium from  $\text{CdWO}_4$  melt, or molybdenum from  $\text{Li}_2\text{MoO}_4$ ,  $\text{CaMoO}_4$ ,  $\text{ZnMoO}_4$ ), which leads to violation of stoichiometry of the melt. Besides, one could expect some influence of growing process to radioactive contamination of crystal scintillators, which effects were never systematically studied. One could expect that at a certain stage of such an R&D, development of special low background growth facilities will be necessary. An interesting R&D was performed in [252] aiming at development of highly radiopure NaI(Tl) crystal scintillators. Authors observed a significant improvement of the crystal radiopurity level by utilization of high purity graphite crucible. Investigations of ceramics used in the growing set-ups was performed in the framework of radiopure  $\text{ZnWO}_4$  crystal scintillators R&D [156]. We would like to stress that the low-thermal gradient Czochralski crystal growth method provides high quality large volume radiopure crystal scintillators [293]. The technique is especially suitable for enriched crystal scintillators production [294].

3. Screening at all stages through ultra-low background  $\gamma$ -spectrometry is needed in the production of compounds for crystal growing (choice of raw materials, quality control of purified elements and compounds).

4. All work should be done using highly pure reagents, lab-ware and water. Careful protection from radon should be foreseen (especially in the case of scintillators R&D for dark matter experiments). All chemistry should be done in clean room conditions, and, as far as possible,

in radon free atmosphere.

5. Cosmogenic activation is expected to be one of the most significant sources of background as the low counting technique improves. Therefore, underground facilities for crystal scintillators production could be a natural step to obtain highly radiopure scintillators.

## 6 Conclusions

Scintillation detectors are widely used to search for rare processes in nuclear and astroparticle physics. Radioactive contamination of scintillation materials can be measured by indirect (inductively coupled plasma mass spectrometry and neutron activation are the most sensitive approaches) and direct (first of all, by low-background HP Ge  $\gamma$  spectrometry) methods. However, the most sensitive method to measure internal contamination of a scintillator are low background measurements when the scintillator operates as a detector. Time-amplitude analysis allows to detect at the  $\mu\text{Bq/kg}$  level the fast sub-chains of the  $^{232}\text{Th}$ ,  $^{235}\text{U}$  and  $^{238}\text{U}$  families which are in equilibrium with  $^{228}\text{Th}$  (from the  $^{232}\text{Th}$  family),  $^{226}\text{Ra}$  ( $^{238}\text{U}$ ) and  $^{227}\text{Ac}$  ( $^{235}\text{U}$ ). Alpha active nuclides can be determined by using pulse-shape discrimination technique. Estimation of  $\beta$  active nuclides can be done by fit of measured energy spectra using Monte Carlo simulated models of background.

Liquid scintillators are the most radiopure scintillation materials with the best up to date achieved residual radioactive contamination level of  $\text{nBq/kg} - \text{pBq/kg}$ . Radioactive contamination of crystal scintillators varies in a wide range. The most radiopure crystal scintillators are  $\text{ZnWO}_4$ ,  $\text{CdWO}_4$ ,  $\text{Li}_2\text{MoO}_4$ ,  $\text{ZnMoO}_4$ ,  $\text{ZnSe}$  and specially developed for dark matter experiments  $\text{NaI(Tl)}$  and  $\text{CsI(Tl)}$  those radioactive contamination by  $^{228}\text{Th}$  and  $^{226}\text{Ra}$  does not exceed the level of  $\sim 0.01 \text{ mBq/kg}$ . Main sources of internal radioactivity of scintillators are daughters of U/Th families,  $^{40}\text{K}$ , radioactive isotopes of elements which are part of a scintillator composition. Scintillation materials containing rare earth elements have comparatively high level of U/Th contamination. Equilibrium of the  $^{232}\text{Th}$ ,  $^{235}\text{U}$  and  $^{238}\text{U}$  chains is usually broken in scintillators.

Next generation  $2\beta$  and dark matter experiments call for extremely low ( $\sim 0.1 - 1 \mu\text{Bq/kg}$ ) level of radioactive contamination of crystal scintillators, that can be obtained in the framework of special programmes that should include deep purification of raw materials, careful screening at all the stages, application of double crystallization. The programmes should involve use of radiopure reagents, lab-ware, equipment and installations, production of raw materials, crystal growing and their storage in radon free atmosphere. Special efforts are necessary to prevent cosmogenic and neutron activation of materials. Development of special underground low background growth facilities may be necessary to reach a further progress in production of radiopure crystal scintillators. Tests of crystal scintillators radioactive contamination on the  $0.1 - 1 \mu\text{Bq/kg}$  level can be realized by ultra-low background direct measurements when a scintillator serves as a detector of its internal radioactivity. The technique of cryogenic scintillating bolometers provides the highest sensitivity to  $\alpha$  active contaminations of crystal scintillators.

## Acknowledgments

F.A. Danevich gratefully acknowledges support from the Jean d'Alembert fellowship program (project CYGNUS) of the Paris-Saclay Excellence Initiative, grant number ANR-10-IDEX-

0003-02. Authors were supported in part by the IDEATE International Associated Laboratory (LIA), and by the project “Investigation of neutrino and weak interaction in double beta decay of  $^{100}\text{Mo}$ ” in the framework of the Programme “Dnipro” based on Ukraine-France Agreement on Cultural, Scientific and Technological Cooperation.

## References

- [1] R. Bernabei, Physics and astrophysics with low background scintillators, *Eur. Phys. J. Spec. Top.* **163**, 207 (2008).
- [2] R. Bernabei et al., Liquid noble gases for dark matter searches: An updated survey, *Int. J. Mod. Phys. A* **30**, 1530053 (2015).
- [3] E. Aprile, T. Doke, Liquid xenon detectors for particle physics and astrophysics, *Rev. Mod. Phys.* **82**, 2053 (2010).
- [4] R.N. Mohapatra et al., Theory of neutrinos: A white paper, *Rep. Prog. Phys.* **70**, 1757 (2007).
- [5] G.L. Fogli et al., Global analysis of neutrino masses, mixings, and phases: Entering the era of leptonic  $CP$  violation searches, *Phys. Rev. D* **86**, 013012 (2012).
- [6] M.C. Gonzalez-Garcia, M. Maltoni, T. Schwetz, Global analyses of neutrino oscillation experiments, *Nucl. Phys. B* **908**, 199 (2016).
- [7] F. Vissani, Global analyses of neutrino oscillation experiments, *Nucl. Phys. At. Energy* **18**, 5 (2017).
- [8] J. Schechter, J.W.F. Valle, Neutrinoless double- $\beta$  decay in  $SU(2)\times U(1)$  theories, *Phys. Rev. D* **25**, 2951 (1982).
- [9] J. Barea, J. Kotila, F. Iachello, Limits on Neutrino Masses from Neutrinoless Double- $\beta$  Decay, *Phys. Rev. Lett.* **109**, 042501 (2012).
- [10] W. Rodejohann, Neutrinoless double-beta decay and neutrino physics, *J. Phys. G: Nucl. Part. Phys.* **39**, 124008 (2012).
- [11] F.F. Deppisch, M. Hirsch, H. Päs, Neutrinoless double-beta decay and physics beyond the standard model, *J. Phys. G: Nucl. Part. Phys.* **39**, 124007 (2012).
- [12] S.M. Bilenky, C. Giunti, Neutrinoless double-beta decay: A probe of physics beyond the Standard Model, *Int. J. Mod. Phys. A* **30**, 1530001 (2015).
- [13] S. Dell’Oro, S. Marcocci, M. Viel, F. Vissani, Neutrinoless Double Beta Decay: 2015 Review, *AHEP* **2016**, 2162659 (2016).
- [14] J.D. Vergados, H. Ejiri, F. Šimkovic, Neutrinoless double beta decay and neutrino mass, *Int. J. Mod. Phys. E* **25**, 1630007 (2016).
- [15] S.R. Elliott, Recent progress in double beta decay, *Mod. Phys. Lett. A* **27**, 1230009 (2012).
- [16] A. Giuliani, A. Poves, Neutrinoless Double-Beta Decay, *AHEP* **2012**, 857016 (2012).
- [17] O. Cremonesi, M. Pavan, Challenges in Double Beta Decay, *AHEP* **2014**, 951432 (2014).

- [18] J.J. Gómez-Cadenas, J. Martín-Albo, Phenomenology of Neutrinoless Double Beta Decay, in *Proc. Gran Sasso Summer Institute 2014 Hands-On Experimental Underground Physics at LNGS (GSSI14)*, INFN – Laboratori Nazionali del Gran Sasso, Assergi, Italy, 22 September – 03 October 2014, *PoS (GSSI14)* 004.
- [19] X. Sarazin, Review of Double Beta Experiments, *J. Phys.: Conf. Ser.* **593**, 012006 (2015).
- [20] H. Pas, W. Rodejohann, Neutrinoless double beta decay, *New J. Phys.* **17**, 115010 (2015).
- [21] M. Agostini et al., Background-free search for neutrinoless double- $\beta$  decay of  $^{76}\text{Ge}$  with GERDA, *Nature* **544**, 47 (2017).
- [22] J.B. Albert et al., Search for Majorana neutrinos with the first two years of EXO-200 data, *Nature* **510**, 229 (2014).
- [23] K. Alfonso et al., Search for Neutrinoless Double-Beta Decay of  $^{130}\text{Te}$  with CUORE-0, *Phys. Rev. Lett.* **115**, 102502 (2015).
- [24] R. Arnold et al., Results of the search for neutrinoless double- $\beta$  decay in  $^{100}\text{Mo}$  with the NEMO-3 experiment, *Phys. Rev. D* **92**, 072011 (2015).
- [25] A. Gando et al., Search for Majorana Neutrinos Near the Inverted Mass Hierarchy Region with KamLAND-Zen, *Phys. Rev. Lett.* **117**, 082503 (2016).
- [26] J. Engel, J. Menéndez, Status and future of nuclear matrix elements for neutrinoless double-beta decay: a review, *Rep. Prog. Phys.* **80**, 046301 (2017).
- [27] A. Giuliani, F.A. Danevich, V.I. Tretyak, A multi-isotope  $0\nu 2\beta$  bolometric experiment, *Eur. Phys. J. C* **78**, 272 (2018).
- [28] E. der Mateosian, M. Goldhaber, Limits for Lepton-Conserving and Lepton-Nonconserving Double Beta Decay in  $\text{Ca}^{48}$ , *Phys. Rev.* **146**, 810 (1966).
- [29] G. Angloher et al., New limits on double electron capture of  $^{40}\text{Ca}$  and  $^{180}\text{W}$ , *J. Phys. G: Nucl. Part. Phys.* **43**, 095202 (2016).
- [30] P. Belli et al., New limits on spin-dependent coupled WIMPs and on  $2\beta$  processes in  $^{40}\text{Ca}$  and  $^{46}\text{Ca}$  by using low radioactive  $\text{CaF}_2(\text{Eu})$  crystal scintillators, *Nucl. Phys. B* **563**, 97 (1999).
- [31] S. Umehara et al., Neutrino-less double- $\beta$  decay of  $^{48}\text{Ca}$  studied by  $\text{CaF}_2(\text{Eu})$  scintillators, *Phys. Rev. C* **78**, 058501 (2008).
- [32] P. Belli et al., Final results of an experiment to search for  $2\beta$  processes in zinc and tungsten with the help of radiopure  $\text{ZnWO}_4$  crystal scintillators, *J. Phys. G: Nucl. Part. Phys.* **38**, 115107 (2011).
- [33] O. Azzolini et al., First Result on the Neutrinoless Double Beta Decay of  $^{82}\text{Se}$  with CUPID-0, arXiv:1802.07791 [nucl-ex].
- [34] L. Cardani et al., First bolometric measurement of the two neutrino double beta decay of  $^{100}\text{Mo}$  with a  $\text{ZnMoO}_4$  crystals array, *J. Phys. G: Nucl. Part. Phys.* **41**, 075204 (2014).

- [35] E. Armengaud et al., Development of  $^{100}\text{Mo}$ -containing scintillating bolometers for a high-sensitivity neutrinoless double-beta decay search, *Eur. Phys. J. C* **77**, 785 (2017).
- [36] D.V. Poda et al.,  $^{100}\text{Mo}$ -enriched  $\text{Li}_2\text{MoO}_4$  scintillating bolometers for  $0\nu 2\beta$  decay search: From LUMINEU to CUPID-0/Mo projects, *AIP Conf. Proc.* **1894**, 020017 (2017).
- [37] J.H. So et al., Scintillation properties and internal background study of  $^{40}\text{Ca}^{100}\text{MoO}_4$  crystal scintillators for neutrino-less double beta decay search, *IEEE Trans. Nucl. Sci.* **59**, 2214 (2012).
- [38] P. Belli et al., Search for  $2\beta$  decay of  $^{106}\text{Cd}$  with an enriched  $^{106}\text{CdWO}_4$  crystal scintillator in coincidence with four HPGe detectors, *Phys. Rev. C* **93**, 045502 (2016).
- [39] P. Belli et al., Search for double- $\beta$  decay processes in  $^{106}\text{Cd}$  with the help of a  $^{106}\text{CdWO}_4$  crystal scintillator, *Phys. Rev. C* **85**, 044610 (2012).
- [40] P. Belli et al., Search for double- $\beta$  decay processes in  $^{108}\text{Cd}$  and  $^{114}\text{Cd}$  with the help of the low-background  $\text{CdWO}_4$  crystal scintillator, *Eur. Phys. J. A* **36**, 167 (2008).
- [41] O.G. Polischuk et al., Investigation of  $2\beta$  Decay of  $^{116}\text{Cd}$  with the Help of Enriched  $^{116}\text{CdWO}_4$  Crystal Scintillators, *AIP Conf. Proc.* **1894**, 020018 (2017).
- [42] R. Cerulli et al., Performances of a  $\text{BaF}_2$  detector and its application to the search for  $\beta\beta$  decay modes in  $^{130}\text{Ba}$ , *Nucl. Instr. Meth. A* **525**, 535 (2004).
- [43] P. Belli et al., Search for  $2\beta$  decay of cerium isotopes with  $\text{CeCl}_3$  scintillator, *J. Phys. G: Nucl. Part. Phys.* **38**, 015103 (2011).
- [44] F.A. Danevich et al., Quest for double beta decay of  $^{160}\text{Gd}$  and Ce isotopes, *Nucl. Phys. A* **694**, 375 (2001).
- [45] F.A. Danevich et al., Search for  $2\beta$  decay of cadmium and tungsten isotopes: Final results of the Solotvina experiment, *Phys. Rev. C* **68**, 035501 (2003).
- [46] M.C. Chen, The SNO Liquid Scintillator Project, *Nucl. Phys. B (Proc. Suppl)* **145**, 65 (2005).
- [47] V. Lozza, on behalf of the SNO+ Collaboration, The SNO+ Experiment for Neutrinoless Double-Beta Decay, *Nucl. Part. Phys. Proc.* **273-275**, 1836 (2016).
- [48] S. Yoshida et al., CANDLES project for double beta decay of  $^{48}\text{Ca}$ , *Nucl. Phys. B (Proc. Suppl.)* **138**, 214 (2005).
- [49] F. Piquemal, The SuperNEMO project, *Phys. Atom. Nucl.* **69**, 2096 (2006).
- [50] A.S. Barabash et al., Calorimeter development for the SuperNEMO double beta decay experiment, *Nucl. Inst. Meth. A* **868**, 98 (2017).
- [51] A. Alessandrello et al., A scintillating bolometer for experiments on double beta decay, *Phys. Lett. B* **420**, 109 (1998).

- [52] S. Pirro et al., Scintillating double-beta-decay bolometers, *Phys. Atom. Nucl.* **69**, 2109 (2006).
- [53] P. Gorla et al., Scintillating bolometers for double beta decay search, *J. Low Temp. Phys.* **151**, 854 (2008).
- [54] S. Pirro, P. Mauskopf, Advances in Bolometer Technology for Fundamental Physics, *Annu. Rev. Nucl. Part. Sci.* **67**, 161 (2017).
- [55] D. Poda, A. Giuliani, Low background techniques in bolometers for double-beta decay search, *Int. J. Mod. Phys. A* **32**, 1743012 (2017).
- [56] V. Alenkov et al., Technical Design Report for the AMoRE  $0\nu 2\beta$  Decay Search Experiment, arXiv:1512.05957v1 [physics.ins-det].
- [57] G. Wang et al., CUPID: CUORE (Cryogenic Underground Observatory for Rare Events) Upgrade with Particle IDentification, arXiv:1504.03599v1 [physics.ins-det].
- [58] G. Wang et al., R&D towards CUPID (CUORE Upgrade with Particle IDentification), arXiv:1504.03612v1 [physics.ins-det].
- [59] C. Arnaboldi et al., Characterization of ZnSe scintillating bolometers for Double Beta Decay, *Astropart. Phys.* **34**, 344 (2011).
- [60] J.W. Beeman et al., Performances of a large mass ZnSe bolometer to search for rare events, *JINST* **8**, P05021 (2013).
- [61] N. Casali et al., Scintillating bolometric technique for the neutrino-less double beta decay search: The LUCIFER/CUPID-0 experiment, *Nucl. Instr. Meth. A* **845**, 342 (2017).
- [62] T.B. Bekker et al., Aboveground test of an advanced  $\text{Li}_2\text{MoO}_4$  scintillating bolometer to search for neutrinoless double beta decay of  $^{100}\text{Mo}$ , *Astropart. Phys.* **72**, 38 (2016).
- [63] S.J. Lee et al., The development of a cryogenic detector with  $\text{CaMoO}_4$  crystals for neutrinoless double beta decay search, *Astropart. Phys.* **34**, 732 (2011).
- [64] G.B. Kim et al., A  $\text{CaMoO}_4$  Crystal Low Temperature Detector for the AMoRE Neutrinoless Double Beta Decay Search, *AHEP* **2015**, 817530 (2015).
- [65] C. Arnaboldi et al.,  $\text{CdWO}_4$  scintillating bolometer for Double Beta Decay: Light and heat anticorrelation, light yield and quenching factors, *Astropart. Phys.* **34**, 143 (2010).
- [66] D.R. Artusa et al., Exploring the neutrinoless double beta decay in the inverted neutrino hierarchy with bolometric detectors, *Eur. Phys. J. C* **74**, 3096 (2014).
- [67] A.S. Barabash et al., First test of an enriched  $^{116}\text{CdWO}_4$  scintillating bolometer for neutrinoless double-beta-decay searches, *Eur. Phys. J. C* **76**, 487 (2016).
- [68] J.W. Beeman et al., A next-generation neutrinoless double beta decay experiment based on  $\text{ZnMoO}_4$  scintillating bolometers, *Phys. Lett. B* **710**, 318 (2012).

- [69] J.W. Beeman et al., ZnMoO<sub>4</sub>: A promising bolometer for neutrinoless double beta decay searches, *Astropart. Phys.* **35**, 813 (2012).
- [70] N.V. Bashmakova et al., Li<sub>2</sub>Zn<sub>2</sub>(MoO<sub>4</sub>)<sub>3</sub> as a potential detector for <sup>100</sup>Mo 2β search, *Functional Materials* **16**, 266 (2009).
- [71] F.A. Danevich et al., Growth and characterization of a Li<sub>2</sub>Mg<sub>2</sub>(MoO<sub>4</sub>)<sub>3</sub> scintillating bolometer, *Nucl. Instr. Meth. A* **889**, 89 (2018).
- [72] D.A. Spassky et al., Luminescent, optical and electronic properties of Na<sub>2</sub>Mo<sub>2</sub>O<sub>7</sub> single crystals, *J. Lumin.* **192**, 1264 (2017).
- [73] V.B. Mikhailik et al., Temperature dependence of scintillation properties of SrMoO<sub>4</sub>, *Nucl. Instr. Meth. A* **792**, 1 (2015).
- [74] K. Zuber, Nd double beta decay search with SNO+, *AIP Conf. Proc.* **942**, 101 (2007).
- [75] S. Umehara et al., Search for Neutrino-less Double Beta Decay with CANDLES, *Phys. Proc.* **61**, 283 (2015).
- [76] A. Luqman et al., Simulations of background sources in AMoRE-I experiment, *Nucl. Instr. Meth. Phys. A* **855**, 140 (2017).
- [77] G. Bertone, D. Hooper, J. Silk, Particle dark matter: evidence, candidates and constraints, *Phys. Rept.* **405**, 279 (2005).
- [78] F.D. Steffen, Dark-matter candidates, *Eur. Phys. J. C* **59**, 557 (2009).
- [79] J.L. Feng, Dark matter candidates from particle physics and methods of detection, *Annu. Rev. Astron. Astrophys.* **48**, 495 (2010).
- [80] J. Bramante et al., Towards the final word on neutralino dark matter, *Phys. Rev. D* **93**, 063525 (2016).
- [81] B.-L. Young, A survey of dark matter and related topics in cosmology, *Front. Phys.* **12**, 121201 (2017).
- [82] R. Bernabei et al., Final model independent results of DAMA/LIBRA - phase 1, *Eur. Phys. J. C* **73**, 2648 (2013).
- [83] L. Baudis et al., First results from the Heidelberg dark matter search experiment, *Phys. Rev. D* **63**, 022001 (2000).
- [84] A. Morales et al., Improved constraints on WIMPs from the international germanium experiment IGEX, *Phys. Lett. B* **532**, 8 (2002).
- [85] C.E. Aalseth et al., Experimental Constraints on a Dark Matter Origin for the DAMA Annual Modulation Effect, *Phys. Rev. Lett.* **101**, 251301 (2008).
- [86] S.T. Lin et al., New limits on spin-independent and spin-dependent couplings of low-mass WIMP dark matter with a germanium detector at a threshold of 220 eV, *Phys. Rev. D* **79**, 061101 (2009).

- [87] W. Zhao et al., Search of low-mass WIMPs with a  $p$ -type point contact germanium detector in the CDEX-1 experiment, *Phys. Rev. D* **93**, 092003 (2016).
- [88] V.N. Lebedenko et al., Result from the first science run of the ZEPLIN-III dark matter search experiment, *Phys. Rev. D* **80**, 052010 (2009).
- [89] J. Angle et al., First Dark Matter Results from the XENON100 Experiment, *Phys. Rev. Lett.* **105**, 131302 (2010).
- [90] P. Benetti et al., First results from a dark matter search with liquid argon at 87 K in the Gran Sasso underground laboratory, *Astropart. Phys.* **28**, 495 (2008).
- [91] K. Abe et al., XMASS detector, *Nucl. Instr. Meth. A* **716**, 78 (2013).
- [92] E. Aprile et al., First Dark Matter Search Results from the XENON1T Experiment, *Phys. Rev. Lett.* **119**, 181301 (2017).
- [93] A. Tan et al., Dark Matter Results from First 98.7 Days of Data from the PandaX-II Experiment, *Phys. Rev. Lett.* **117**, 121303 (2016).
- [94] D.S. Akerib et al., Results from a Search for Dark Matter in the Complete LUX Exposure, *Phys. Rev. Lett.* **118**, 021303 (2017).
- [95] J. Calvo et al., Commissioning of the ArDM experiment at the Canfranc underground laboratory: first steps towards a tonne-scale liquid argon time projection chamber for Dark Matter searches, *JCAP* **03**, 003 (2017).
- [96] C. Amole et al., Dark Matter Search Results from the PICO-60 C<sub>3</sub>F<sub>8</sub> Bubble Chamber, *Phys. Rev. Lett.* **118**, 251301 (2017).
- [97] V. Sanglard et al., Final results of the EDELWEISS-I dark matter search with cryogenic heat-and-ionization Ge detectors, *Phys. Rev. D* **71**, 122002 (2005).
- [98] Z. Ahmed et al., Search for Weakly Interacting Massive Particles with the First Five-Tower Data from the Cryogenic Dark Matter Search at the Soudan Underground Laboratory, *Phys. Rev. Lett.* **102**, 011301 (2009).
- [99] R. Agnese et al., New Results from the Search for Low-Mass Weakly Interacting Massive Particles with the CDMS Low Ionization Threshold Experiment, *Phys. Rev. Lett.* **116**, 071301 (2016).
- [100] R. Bernabei et al., Search for WIMP annual modulation signature: results from DAMA/NaI-3 and DAMA/NaI-4 and the global combined analysis, *Phys. Lett. B* **480**, 23 (2000).
- [101] G.J. Alner et al., Limits on WIMP cross-sections from the NAIAD experiment at the Boulby Underground Laboratory, *Phys. Lett. B* **616**, 17 (2005).
- [102] S.C. Kim et al., New Limits on Interactions between Weakly Interacting Massive Particles and Nucleons Obtained with CsI(Tl) Crystal Detectors, *Phys. Rev. Lett.* **108**, 181301 (2012).

- [103] P. Belli, A. Incicchitti, F. Cappella, Inorganic scintillators in direct dark matter investigation, *Int. J. Mod. Phys. A* **29**, 1443011 (2014).
- [104] G. Angloher et al., Results on light dark matter particles with a low-threshold CRESST-II detector, *Eur. Phys. J. C* **76**, 25 (2016).
- [105] F. Petricca et al., First results on low-mass dark matter from the CRESST-III experiment, arXiv:1711.07692v1 [astro-ph.CO].
- [106] E. Shields, J. Xu, F. Calaprice, SABRE: A new NaI(Tl) dark matter direct detection experiment, *Phys. Procedia* **61**, 169 (2015).
- [107] J. Amaré et al., Status of the ANAIS Dark Matter Project at the Canfranc Underground Laboratory, *J. Phys.: Conf. Ser.* **718**, 042052 (2016).
- [108] K. Fushimi et al., Dark matter search project PICO-LON, *J. Phys.: Conf. Ser.* **718**, 042022 (2016).
- [109] E. Barbosa de Souza et al., First search for a dark matter annual modulation signal with NaI(Tl) in the Southern Hemisphere by DM-Ice17, *Phys. Rev. D* **95**, 032006 (2017).
- [110] G. Adhikari et al., Initial Performance of the COSINE-100 Experiment, *Eur. Phys. J. C* **78**, 107 (2018).
- [111] G. Angloher et al., The COSINUS project: perspectives of a NaI scintillating calorimeter for dark matter search, *Eur. Phys. J. C* **76**, 441 (2016).
- [112] G. Angloher et al., A CsI low-temperature detector for dark matter search, *Astropart. Phys.* **84**, 70 (2016).
- [113] T. Iida, Multi purpose detector using high light yield  $\text{CaI}_2$  crystal, 15th International Conference on Topics in Astroparticle and Underground Physics TAUP 2017, 24 - 28 July 2017, Sudbury, ON, Canada.
- [114] K. Kamada et al., Single crystal growth and scintillation properties of  $\text{Ca}(\text{Cl}, \text{Br}, \text{I})_2$  single crystal, *Ceram. Int.* **43**, S423 (2017).
- [115] F. Cappella et al., On the potentiality of the  $\text{ZnWO}_4$  anisotropic detectors to measure the directionality of Dark Matter, *Eur. Phys. J. C* **73**, 2276 (2013)
- [116] R. Cerulli, Low background techniques toward a  $\text{ZnWO}_4$  directionality experiment, *Int. J. Mod. Phys. A* **32**, 1743009 (2017).
- [117] S. Cebrián, Cosmogenic activation of materials, *Int. J. Mod. Phys. A* **32**, 1743006 (2017).
- [118] F. Capozzi et al., Neutrino masses and mixings: Status of known and unknown  $3\nu$  parameters, *Nucl. Phys. B* **908**, 218 (2016).
- [119] X. Qiana, P. Vogel, Neutrino mass hierarchy, *Prog. Part. Nucl. Phys.* **83**, 1 (2015).
- [120] P.F. de Salas et al., Status of neutrino oscillations 2017, arXiv:1708.01186v1 [hep-ph].

- [121] O. Smirnov et al., Solar neutrino with Borexino: Results and perspectives, *Phys. Part. Nucl.* **46**, 166 (2015).
- [122] S. Abe et al., Precision Measurement of Neutrino Oscillation Parameters with KamLAND, *Phys. Rev. Lett.* **100**, 221803 (2008).
- [123] P. Vogel, L.J. Wen, C. Zhang, Neutrino oscillation studies with reactors, *Nat. Commun.* **6**, 6935 (2015).
- [124] F.P. An et al., Observation of Electron-Antineutrino Disappearance at Daya Bay, *Phys. Rev. Lett.* **108**, 171803 (2012).
- [125] Y. Abe et al., Measurement of  $\theta_{13}$  in Double Chooz using neutron captures on hydrogen with novel background rejection techniques, *JHEP* **01**, 163 (2016).
- [126] J.H. Choi et al., Observation of Energy and Baseline Dependent Reactor Antineutrino Disappearance in the RENO Experiment, *Phys. Rev. Lett.* **116**, 211801 (2016).
- [127] F. An et al., Neutrino physics with JUNO, *J. Phys. G: Nucl. Part. Phys.* **43**, 030401 (2016).
- [128] G. Ranucci and JUNO Collaboration, Status and prospects of the JUNO experiment, *J. Phys.: Conf. Ser.* **888**, 012022 (2017).
- [129] T. Adam et al., JUNO Conceptual Design Report, arXiv:1508.07166v2 [physics.ins-det].
- [130] H. Ejiri, H. Kinoshita, H. Sano, H. Ohsumi, Search for exotic K X-rays from neutral iodine atoms and limits on charge non-conservation, *Phys. Lett. B* **282**, 281 (1992).
- [131] P. Belli et al., New experimental limit on the electron stability and non-paulian transitions in Iodine atoms, *Phys. Lett. B* **460**, 236 (1999).
- [132] R. Bernabei et al., New search for processes violating the Pauli exclusion principle in sodium and in iodine, *Eur. Phys. J. C* **62**, 327 (2009).
- [133] P. Belli et al., New limits on the nuclear levels excitation of  $^{127}\text{I}$  and  $^{23}\text{Na}$  during charge nonconservation, *Phys. Rev. C* **60**, 065501 (1999).
- [134] R. Bernabei et al., Search for the nucleon and di-nucleon decay into invisible channels, *Phys. Lett. B* **493**, 12 (2000).
- [135] P. Belli et al., New experimental limits on the electron stability and excitation of nuclear levels in  $^{23}\text{Na}$ ,  $^{127}\text{I}$  and  $^{129}\text{Xe}$  induced by the electron decay on the atomic shell, *Part. Nucl. Lett.* **6**, 58 (2001).
- [136] P. Belli et al., Search for solar axions by Primakoff effect in NaI crystals, *Phys. Lett. B* **515**, 6 (2001).
- [137] H.O. Back et al., New limits on nucleon decays into invisible channels with the BOREXINO counting test facility, *Phys. Lett. B* **563**, 23 (2003).

- [138] M. Agostini et al., Limiting neutrino magnetic moments with Borexino Phase-II solar neutrino data, *Phys. Rev. D* **96**, 091103 (2017).
- [139] G. Bellini et al., Search for solar axions emitted in the M1-transition of  ${}^7\text{Li}^*$  with Borexino CTF, *Eur. Phys. J. C* **54**, 61 (2008).
- [140] G. Bellini et al., Search for solar axions produced in the  $p(d, {}^3\text{He})\text{A}$  reaction with Borexino detector, *Phys. Rev. D* **85**, 092003 (2012).
- [141] G. Bellini et al., New experimental limits on the Pauli-forbidden transitions in  ${}^{12}\text{C}$  nuclei obtained with 485 days Borexino data, *Phys. Rev. C* **81**, 034317 (2010).
- [142] S.N. Ahmed et al., Constraints on Nucleon Decay via Invisible Modes from the Sudbury Neutrino Observatory, *Phys. Rev. Lett.* **92**, 102004 (2004).
- [143] T. Araki et al., Search for the Invisible Decay of Neutrons with KamLAND, *Phys. Rev. Lett.* **96**, 101802 (2006).
- [144] R. Bernabei et al., Search for possible charge non-conserving decay of  ${}^{139}\text{La}$  into  ${}^{139}\text{Ce}$  with  $\text{LaCl}_3(\text{Ce})$  scintillator, *Ukr. J. Phys.* **51**, 1037 (2006).
- [145] A. Alessandrello et al., Bolometric measurement of the beta spectrum of  ${}^{113}\text{Cd}$ , *Nucl. Phys. B (Proc. Suppl.)* **35**, 394 (1994).
- [146] F.A. Danevich et al., Beta decay of  ${}^{113}\text{Cd}$ , *Phys. Atom. Nucl.* **59**, 1 (1996).
- [147] P. Belli et al., Investigation of  $\beta$  decay of  ${}^{113}\text{Cd}$ , *Phys. Rev. C* **76**, 064603 (2007).
- [148] K. Kossert, Half-life measurement of  ${}^{87}\text{Rb}$  by liquid scintillation counting, *Appl. Rad. Isot.* **59**, 377 (2003).
- [149] L. Pfeiffer et al., Beta spectrum of  ${}^{115}\text{In}$ , *Phys. Rev. C* **19**, 1035 (1979).
- [150] L. Pattavina et al., An innovative technique for the investigation of the 4-fold forbidden beta-decay of  ${}^{50}\text{V}$ , arXiv:1801.03980 [physics.ins-det].
- [151] G.B. Beard, W.H. Kelly, Search for the natural alpha activity of tungsten, *Nucl. Phys.* **16**, 591 (1960).
- [152] A.Sh. Georgadze et al., Search for  $\alpha$  decay of naturally occurring tungsten isotopes, *JETP Lett.* **61**, 882 (1995).
- [153] F.A. Danevich et al.,  $\alpha$  activity of natural tungsten isotopes, *Phys. Rev. C* **67**, 014310 (2003).
- [154] C. Cozzini et al., Detection of the natural  $\alpha$  decay of tungsten, *Phys. Rev. C* **70**, 064606 (2004).
- [155] Yu.G. Zdesenko et al., Scintillation properties and radioactive contamination of  $\text{CaWO}_4$  crystal scintillators, *Nucl. Instr. Meth. A* **538**, 657 (2005).

- [156] P. Belli et al., Radioactive contamination of ZnWO<sub>4</sub> crystal scintillators, *Nucl. Instr. Meth. A* **626-627**, 31 (2011).
- [157] P. de Marcillac et al., Experimental detection of  $\alpha$ -particles from the radioactive decay of natural bismuth, *Nature* **422**, 876 (2003).
- [158] J.W. Beeman et al., First Measurement of the Partial Widths of <sup>209</sup>Bi Decay to the Ground and to the First Excited States, *Phys. Rev. Lett.* **108**, 062501 (2012).
- [159] P. Belli et al., Search for  $\alpha$  decay of natural Europium, *Nucl. Phys. A* **789**, 15 (2007).
- [160] N. Casali et al., Discovery of the <sup>151</sup>Eu  $\alpha$  decay, *J. Phys. G: Nucl. Part. Phys.* **41**, 075101 (2014).
- [161] J.W. Beeman et al., New experimental limits on the  $\alpha$  decays of lead isotopes, *Eur. Phys. J. A* **49**, 50 (2013).
- [162] N. Casali et al., Cryogenic Detectors for Rare Alpha Decay Search: A New Approach, *J. Low Temp. Phys.* **184**, 952 (2016).
- [163] N. Coron et al., Measurement of the L/K electron capture ratio of the <sup>207</sup>Bi decay to the 1633 keV level of <sup>207</sup>Pb with a BGO scintillating bolometer, *Eur. Phys. J. A* **48**, 89 (2012).
- [164] R. Bernabei et al., New search for correlated e<sup>+</sup>e<sup>-</sup> pairs in the decay of <sup>241</sup>Am, *Eur. Phys. J. A* **49**, 64 (2013).
- [165] <https://www.nndc.bnl.gov/ensdf>
- [166] J. Meija et al., Isotopic compositions of the elements 2013 (IUPAC Technical Report), *Pure Appl. Chem.* **88**, 293 (2016).
- [167] J. Meija et al., Atomic weights of the elements 2013 (IUPAC Technical Report), *Pure Appl. Chem.* **88**, 265 (2016).
- [168] R. Arnold et al., Measurement of the double-beta decay half-life and search for the neutrinoless double-beta decay of <sup>48</sup>Ca with the NEMO-3 detector, *Phys. Rev. D* **93**, 112008 (2016).
- [169] H. Dombrowski, S. Neumaier, K. Zuber, Precision half-life measurement of the 4-fold forbidden  $\beta$  decay of <sup>50</sup>V, *Phys. Rev. C* **83**, 054322 (2011).
- [170] M. Agostini et al., Results on  $\beta\beta$  decay with emission of two neutrinos or Majorons in <sup>76</sup>Ge from GERDA Phase I, *Eur. Phys. J. C* **75**, 416 (2015).
- [171] R. Arnold et al., First Results of the Search for Neutrinoless Double-Beta Decay with the NEMO 3 Detector, *Phys. Rev. Lett.* **95**, 182302 (2005).
- [172] J. Argyriades et al., Measurement of the two neutrino double beta decay half-life of Zr-96 with the NEMO-3 detector, *Nucl. Phys. A* **847**, 168 (2010).

- [173] A.S. Barabash, Average and recommended half-life values for two-neutrino double beta decay, *Nucl. Phys. A* **935**, 52 (2015).
- [174] C. Alduino et al., Measurement of the two-neutrino double-beta decay half-life of  $^{130}\text{Te}$  with the CUORE-0 experiment, *Eur. Phys. J. C* **77**, 13 (2017).
- [175] R. Arnold et al., Measurement of the  $2\nu\beta\beta$  decay half-life of  $^{150}\text{Nd}$  and a search for  $0\nu\beta\beta$  decay processes with the full exposure from the NEMO-3 detector, *Phys. Rev. D* **94**, 072003 (2016).
- [176] K. Kossert, G.Jörg, C.L. v. Gostomski, Experimental half-life determination of  $^{176}\text{Lu}$ , *Appl. Rad. Isot.* **81**, 140 (2013).
- [177] M. Braun et al., A new precision measurement of the  $\alpha$ -decay half-life of  $^{190}\text{Pt}$ , *Phys. Lett. B* **768**, 317 (2017).
- [178] S. Nici, L. Copia, I. Dafinei, M.L. Di Vacri, ICP-MS measurement of natural radioactivity at LNGS, *Int. J. Mod. Phys. A* **32**, 1743003 (2017).
- [179] I.J. Arnquist., E.W. Hoppe, The quick and ultrasensitive determination of K in NaI using inductively coupled plasma mass spectrometry, *Nucl. Instr. Meth. A* **851**, 15 (2017).
- [180] K.J. Dong et al., Measurement of ultra-low potassium contaminations with Accelerator Mass Spectrometry, *Nucl. Instr. Meth. A* **582**, 381 (2007).
- [181] Z. Djurcic et al., Novel technique for ultra-sensitive determination of trace elements in organic scintillators, *Nucl. Instr. Meth. A* **507**, 680 (2003).
- [182] G. Heusser, Low-radioactivity background techniques, *Ann. Rev. Nucl. Part. Sci.* **45**, 543 (1995).
- [183] P.P. Povinec, Analysis of radionuclides at ultra-low levels: A comparison of low and high energy mass spectrometry with gamma-spectrometry for radiopurity measurements, *Appl. Rad. Isot.* **126**, 26 (2017).
- [184] M. Laubenstein, Screening of materials with high purity germanium detectors at the Laboratori Nazionali del Gran Sasso, *Int. J. Mod. Phys. A* **32**, 1743002 (2017).
- [185] A. Balysh et al., Radioactive impurities in crystals of bismuth germanate, *Pribory i Tekhnika Eksperimenta* **36**, 118 (1993) (in Russian).
- [186] Y.D. Kim et al., Inhibition of  $^{137}\text{Cs}$  contamination in cesium iodide, *Nucl. Instr. Meth. A* **552**, 456 (2005).
- [187] H.S. Lee et al., Development of low background CsI(Tl) crystals for WIMP search, *Nucl. Instr. Meth. A* **571**, 644 (2007).
- [188] E. Picado, L.M. Fraile, I. Bandac, J.M. Udias, Radiopurity study of an encapsulated  $\text{CeBr}_3$  crystal, *JPS Conf. Proc.* **6**, 030133 (2015).
- [189] C. Cardenas et al., Internal contamination of the  $\text{Cs}_2\text{HfCl}_6$  crystal scintillator, *Nucl. Instr. Meth. A* **872**, 23 (2017).

- [190] H. Simgen, G. Heusser, M. Laubenstein, G. Zuzel, Analysis of radioactive trace impurities with  $\mu\text{Bq}$ -sensitivity in Borexino, *Int. J. Mod. Phys. A* **29**, 1442009 (2014).
- [191] P. Belli et al., Intrinsic radioactivity of a  $\text{Li}_6\text{Eu}(\text{BO}_3)_3$  crystal and  $\alpha$  decays of Eu, *Nucl. Instr. Meth. A* **572**, 734 (2007).
- [192] I. Bavykina et al., Development of cryogenic phonon detectors based on  $\text{CaMoO}_4$  and  $\text{ZnWO}_4$  scintillating crystals for direct dark matter search experiments, *Opt. Mater.* **31**, 1382 (2009).
- [193] O.P. Barinova et al., Intrinsic radiopurity of a  $\text{Li}_2\text{MoO}_4$  crystal, *Nucl. Instr. Meth. A* **607**, 573 (2009).
- [194] P. Loaiza et al., Low background germanium planar detector for gamma-ray spectrometry, *Nucl. Instr. Meth. A* **634**, 64 (2011).
- [195] A.S. Barabash et al., Low background detector with enriched  $^{116}\text{CdWO}_4$  crystal scintillators to search for double  $\beta$  decay of  $^{116}\text{Cd}$ , *JINST* **6**, P08011 (2011).
- [196] F.A. Danevich et al., Effect of recrystallisation on the radioactive contamination of  $\text{CaWO}_4$  crystal scintillators. *Nucl. Instr. Meth. A* **631**, 44 (2011).
- [197] P. Belli et al., Radioactive contamination of  $\text{SrI}_2(\text{Eu})$  crystal scintillator, *Nucl. Instr. Meth. A* **670**, 10 (2012).
- [198] P. Belli et al., Radioactive contamination of  $^7\text{LiI}(\text{Eu})$  crystal scintillators, *Nucl. Instr. Meth. A* **704**, 40 (2013).
- [199] F.A. Danevich et al., Search for  $2\beta$  decay of  $^{116}\text{Cd}$  with the help of a  $^{116}\text{CdWO}_4$  scintillator, *JETP Lett.* **49**, 476 (1989).
- [200] H. Ejiri et al., The high sensitivity beta-gamma spectrometer ELEGANTS V for rare  $\beta(e)$  and  $\beta\beta(\text{ee})$  decays, *Nucl. Instr. Meth. A* **302**, 304 (1991).
- [201] F.A. Danevich et al., Investigation of  $\beta^+\beta^+$  and  $\beta^+/\text{EC}$  decay of  $^{106}\text{Cd}$ , *Z. Phys. A* **355**, 433 (1996).
- [202] R. Bernabei et al., Performances of the  $\approx 100$  kg  $\text{NaI}(\text{Tl})$  set-up of the DAMA experiment at Gran Sasso, *Il Nuovo Cimento A* **112**, 545 (1999).
- [203] F.A. Danevich et al., New results of  $^{116}\text{Cd}$  double  $\beta$  decay study with  $^{116}\text{CdWO}_4$  scintillators, *Phys. Rev. C* **62**, 045501 (2000).
- [204] S.C. Wang, H.T. Wong, M. Fujiwara, Measurement of intrinsic radioactivity in a GSO crystal, *Nucl. Instr. Meth. A* **479**, 498 (2002).
- [205] P. Belli et al., Performances of a  $\text{CeF}_3$  crystal scintillator and its application to the search for rare processes, *Nucl. Instr. Meth. A* **498**, 352 (2003).
- [206] I. Ogawa et al., Double beta decay study of  $^{48}\text{Ca}$  by  $\text{CaF}_2$  scintillator, *Nucl. Phys. A* **721**, 525c (2003).

- [207] B. Ahmed et al., The NAIAD experiment for WIMP searches at Boulby mine and recent results, *Astropart. Phys.* **19**, 691 (2003).
- [208] Y.F. Zhu et al., Measurement of the intrinsic radiopurity of  $^{137}\text{Cs}/^{235}\text{U}/^{238}\text{U}/^{232}\text{Th}$  in CsI(Tl) crystal scintillators, *Nucl. Instr. Meth. A* **557**, 490 (2006).
- [209] R. Bernabei et al., The DAMA/LIBRA apparatus, *Nucl. Instr. Meth. A* **592**, 297 (2008).
- [210] F.A. Danevich et al.,  $\text{ZnWO}_4$  crystals as detectors for  $2\beta$  decay and dark matter experiments, *Nucl. Instr. Meth. A* **544**, 553 (2005).
- [211] J.B. Birks, Theory and Practice of Scintillation Counting, Pergamon. London; Macmillan, New York, 1964.
- [212] V.I. Tretyak, Semi-empirical calculation of quenching factors for ions in scintillators, *Astropart. Phys.* **33**, 40 (2010).
- [213] W. Wolszczak, P. Dorenbos, Nonproportional Response of Scintillators to Alpha Particle Excitation, *IEEE Trans. Nucl. Sci.* **64**, 1580 (2017).
- [214] P. Schuster, Investigating the Anisotropic Scintillation Response in Anthracene through Neutron, Gamma-Ray, and Muon Measurements, *IEEE Trans. Nucl. Sci.* **63**, 1942 (2016).
- [215] P. Schuster, E. Brubaker, Characterization of the scintillation anisotropy in crystalline stilbene scintillator detectors, *Nucl. Instr. Meth. A* **859**, 95 (2017).
- [216] F.A. Danevich et al.,  $\text{MgWO}_4$  – A new crystal scintillator, *Nucl. Instr. Meth. A* **608**, 107 (2009).
- [217] M. Wang et al., The Ame2016 atomic mass evaluation, *Chin. Phys. C* **41**, 030003 (2017).
- [218] P.G. Bizzeti et al., Response of  $\text{CdWO}_4$  crystal scintillator for few MeV ions and low energy electrons, *Nucl. Instr. Meth. A* **696**, 144 (2012).
- [219] P. Dorenbos, J.T.M. de Haas, C.W.E. van Eijk, Non-Proportionality in the Scintillation Response and the Energy Resolution Obtainable with Scintillation Crystals, *IEEE Trans. Nucl. Sci.* **42**, 2190 (1995).
- [220] M. Moszynski et al., Energy resolution of scintillation detectors, *Nucl. Instr. Meth. A* **805**, 25 (2016).
- [221] H.O. Back et al., Search for electron decay mode  $e \rightarrow \gamma + \nu$  with prototype of Borexino detector, *Phys. Lett. B* **525**, 29 (2002).
- [222] C. Aberle et al., Light output of Double Chooz scintillators for low energy electrons, *JINST* **06**, P11006 (2011).
- [223] F.A. Danevich et al., The research of  $2\beta$  decay of  $^{116}\text{Cd}$  with enriched  $^{116}\text{CdWO}_4$  crystal scintillators, *Phys. Lett. B* **344**, 72 (1995).
- [224] J.C. Barton, J.A. Edgington, Analysis of alpha-emitting isotopes in an inorganic scintillator, *Nucl. Instr. Meth. A* **443**, 277 (2000).

- [225] E. Gatti, F. De Martini, A new linear method of discrimination of elementary particles in scintillation. counters, *Nuclear Electronics 2*, I.A.E.A., Vienna, 1962, p. 265.
- [226] T. Fazzini et al., Pulse-shape discrimination with  $\text{CdWO}_4$  crystal scintillators, *Nucl. Instr. Meth. A* **410**, 213 (1998).
- [227] F.A. Danevich et al., YAG:Nd crystals as possible detector to search for  $2\beta$  and  $\alpha$  decay of neodymium, *Nucl. Instr. Meth. A* **541**, 583 (2005).
- [228] L. Bardelli et al., Pulse-shape discrimination with  $\text{PbWO}_4$  crystal scintillators, *Nucl. Instr. Meth. A* **584**, 129 (2008).
- [229] A.N. Annenkov et al., Development of  $\text{CaMoO}_4$  crystal scintillators for double beta decay experiment with  $^{100}\text{Mo}$ , *Nucl. Instr. Meth. A* **584**, 334 (2008).
- [230] Yu.G. Zdesenko et al., CARVEL experiment with  $^{48}\text{CaWO}_4$  crystal scintillators for the double  $\beta$  decay study of  $^{48}\text{Ca}$ , *Astropart. Phys.* **23**, 249 (2005).
- [231] S. Agostinelli et al., GEANT4 – A simulation toolkit, *Nucl. Instr. Meth. A* **506**, 250 (2003).
- [232] J. Allison et al., Geant4 developments and applications, *IEEE Trans. Nucl. Sci.* **53**, 270 (2006).
- [233] J. Allison et al., Recent developments in Geant4, *Nucl. Instr. Meth. A* **835**, 186 (2016).
- [234] O.A. Ponkratenko, V.I. Tretyak, Yu.G. Zdesenko, Event generator DECAY4 for simulation of double-beta processes and decays of radioactive nuclei, *Phys. Atom. Nucl.* **63**, 1282 (2000).
- [235] W.R. Nelson, H. Hirayama, D.W.O. Rogers, The EGS4 code system. SLAC Report 265; 1985.
- [236] L. Gironi, Scintillating bolometers for Double Beta Decay search, *Nucl. Instr. Meth. A* **617**, 478 (2010).
- [237] G. Zuzel, Low background techniques applied in the BOREXINO experiment, *AIP Conf. Proc.* **1672**, 110001 (2015).
- [238] G. Keefer, Laboratory Studies of Lead Removal from Liquid Scintillator in Preparation for KamLANDs Low Background Phase, *AIP Conf. Proc.* **1338**, 175 (2011).
- [239] J. Argyriades et al., Results of the BiPo-1 prototype for radiopurity measurements for the SuperNEMO double beta decay source foils, *Nucl. Instr. Meth. A* **622**, 120 (2010).
- [240] G. Heusser et al., GIOVE: a new detector setup for high sensitivity germanium spectroscopy at shallow depth, *Eur. Phys. J. C* **75**, 531 (2015).
- [241] P. Belli et al., Search for  $^7\text{Li}$  solar axions using resonant absorption in LiF crystal: Final results, *Phys. Lett. B* **711**, 41 (2012).

- [242] I. Ogawa et al., Search for neutrino-less double beta decay of  $^{48}\text{Ca}$  by  $\text{CaF}_2$  scintillator, *Nucl. Phys. A* **730**, 215 (2004).
- [243] C.G. Díaz, Characterization of scintillating bolometers for particle detection and installation of a bolometric test facility in the University of Zaragoza, Tesis Doctoral, Universidad de Zaragoza, 2013, Spain.
- [244] P. Belli et al., Investigation of rare nuclear decays with  $\text{BaF}_2$  crystal scintillator contaminated by radium, *Eur. Phys. J. A* **50**, 134 (2014).
- [245] D.R. Artusa et al., First array of enriched  $\text{Zn}^{82}\text{Se}$  bolometers to search for double beta decay, *Eur. Phys. J. C* **76**, 364 (2016).
- [246] J. Amaré et al., Background understanding and improvement in NaI scintillators, *J. Phys.: Conf. Series* **39**, 201 (2006).
- [247] C. Cuesta et al., Analysis of the  $^{40}\text{K}$  contamination in NaI(Tl) crystals from different providers in the frame of the ANAIS project, *Int. J. Mod. Phys. A* **29**, 1443010 (2014).
- [248] J. Amaré et al., Preliminary results of ANAIS-25, *Nucl. Instr. Meth. A* **742**, 187 (2014).
- [249] J. Amaré et al., Background model of NaI(Tl) detectors for the ANAIS Dark Matter Project, arXiv:1508.07907v1 [physics.ins-det].
- [250] J. Amare et al., Assessment of backgrounds of the ANAIS experiment for dark matter direct detection, *Eur. Phys. J. C* **76**, 429 (2016).
- [251] K. Fushimi et al., KamLAND-PICO project to search for cosmic dark matter, arXiv:1407.3542v1 [astro-ph.IM].
- [252] K. Fushimi et al., High purity NaI(Tl) scintillator to search for dark matter, *JPC Conf. Proc.* **11**, 020003 (2016).
- [253] H.S. Lee on behalf of the KIMS Collaboration, Development of low background CsI(Tl) and NaI(Tl) crystals for WIMP search, *AIP Conf. Proc.* **1672**, 040002 (2015).
- [254] K.W. Kim et al., Tests on NaI(Tl) crystals for WIMP search at the Yangyang Underground Laboratory, *Astropart. Phys.* **62**, 249 (2015).
- [255] P. Adhikari et al., Understanding internal backgrounds in NaI(Tl) crystals toward a 200 kg array for the KIMS-NaI experiment, *Eur. Phys. J. C* **76**, 185 (2016).
- [256] J. Cherwinka et al., First data from DM-Ice17, *Phys. Rev. D* **90**, 092005 (2014).
- [257] D. D'Angelo for the SABRE collaboration, SABRE NaI(Tl) Dark Matter Investigation at low Radioactivity, *PoS (NOW2016)* 086.
- [258] G. Adhikari et al., Initial performance of the COSINE-100 experiment, *Eur. Phys. J. C* **78**, 107 (2018).
- [259] S.K. Liu et al., Measurement of intrinsic radioactive backgrounds from the  $^{137}\text{Cs}$  and U/Th chains in CsI(Tl) crystals, *Chin. Phys. C* **39**, 046002 (2015).

- [260] J.I. Collar et al., Coherent neutrino-nucleus scattering detection with a CsI[Na] scintillator at the SNS spallation source, *Nucl. Instr. Meth. A* **773**, 56 (2015).
- [261] R. Bernabei et al., Performances and potentialities of a LaCl<sub>3</sub>:Ce scintillator, *Nucl. Instr. Meth. A* **555**, 270 (2005).
- [262] G. Lutter et al., Radiopurity of a CeBr<sub>3</sub> crystal used as scintillation detector, *Nucl. Instr. Meth. A* **703**, 158 (2013).
- [263] N. Coron et al., Our-short-experience at IAS and within ROSEBUD with radioactive contaminations in scintillating bolometers: uses and needs, presented at the Workshop on Radiopure scintillators for EURECA (RPSCINT 2008), 9-10 September 2008, Kyiv, Ukraine, p. 12, arXiv:0903.1539 [nucl-ex].
- [264] A.Sh. Georgadze et al., Evaluation of activities of impurity radionuclides in cadmium tungstate crystals, *Instr. Exp. Technique* **39**, 191 (1996).
- [265] S.Ph. Burachas et al., Large volume CdWO<sub>4</sub> crystal scintillators, *Nucl. Instr. Meth. A* **369**, 164 (1996).
- [266] P. Belli et al., Development of enriched <sup>106</sup>CdWO<sub>4</sub> crystal scintillators to search for double  $\beta$  decay processes in <sup>106</sup>Cd, *Nucl. Instr. Meth. A* **615**, 301 (2010).
- [267] D.V. Poda et al., CdWO<sub>4</sub> crystal scintillators from enriched isotopes for double beta decay experiments, *Rad. Meas.* **56**, 66 (2013).
- [268] S. Cebrián et al., Bolometric WIMP search at Canfranc with different absorbers, *Astropart. Phys.* **21**, 23 (2004).
- [269] A. Münster et al., Radiopurity of CaWO<sub>4</sub> crystals for direct dark matter search with CRESST and EURECA, *JCAP* **05**, 018 (2014).
- [270] R. Strauss et al., Beta/gamma and alpha backgrounds in CRESST-II Phase 2, *JCAP* **06**, 030 (2015).
- [271] F.A. Danevich et al., Application of PbWO<sub>4</sub> crystal scintillators in experiment to search for  $2\beta$  decay of <sup>116</sup>Cd, *Nucl. Instr. Meth. A* **556**, 259 (2006).
- [272] H.V. Klapdor-Kleingrothaus et al., GENIUS-TF: A test facility for the GENIUS project, *Nucl. Instr. Meth. A* **481**, 149 (2002).
- [273] C. Dörr, H.V. Klapdor-Kleingrothaus, New Monte-Carlo simulation of the HEIDELBERG-MOSCOW double beta decay experiment, *Nucl. Instr. Meth. A* **513**, 596 (2003).
- [274] H. Bhang et al., AMoRE experiment: a search for neutrinoless double beta decay of <sup>100</sup>Mo isotope with <sup>40</sup>Ca<sup>100</sup>MoO<sub>4</sub> cryogenic scintillation detector, *J. Phys.: Conf. Ser.* **375**, 042023 (2012).
- [275] M.X. Xue et al., Study of CdMoO<sub>4</sub> crystal for a neutrinoless double beta decay experiment with <sup>116</sup>Cd and <sup>100</sup>Mo nuclides, *Chin. Phys. C* **41**, 046002 (2017).

- [276] J. Benziger et al., A scintillator purification system for the Borexino solar neutrino detector, *Nucl. Instr. Meth. A* **587**, 277 (2008).
- [277] F. Suekane et al., for the KamLAND RCNS Group, An Overview of the KamLAND 1-kiloton Liquid Scintillator, arXiv:physics/0404071v2 [physics.ins-det].
- [278] L. Miramonti, Low background techniques in liquid scintillator detectors, *Int. J. Mod. Phys. A* **32**, 1743010 (2017).
- [279] R. Bernabei, P. Belli, A. Incicchitti, C.J. Dai, Adopted low background techniques and analysis of radioactive trace impurities, *Int. J. Mod. Phys. A* **31**, 1642003 (2016).
- [280] R. Bernabei, A. Incicchitti, Low background techniques in NaI(Tl) setups, *Int. J. Mod. Phys. A* **32**, 1743007 (2017).
- [281] A.S. Barabash et al., Improvement of radiopurity level of enriched  $^{116}\text{CdWO}_4$  and  $\text{ZnWO}_4$  crystal scintillators by recrystallization, *Nucl. Instr. Meth. A* **833**, 77 (2016).
- [282] J.Y. Lee et al., A Study of Radioactive Contamination of  $^{40}\text{Ca}^{100}\text{MoO}_4$  Crystals for the AMoRE Experiment, *IEEE Trans. Nucl. Sci.* **63**, 543 (2016).
- [283] I. Dafinei et al., Production of  $^{82}\text{Se}$  enriched Zinc Selenide ( $\text{ZnSe}$ ) crystals for the study of neutrinoless double beta decay, *J. Cryst. Growth* **475**, 158 (2017).
- [284] D.M. Chernyak et al., Optical, luminescence and thermal properties of radiopure  $\text{ZnMoO}_4$  crystals used in scintillating bolometers for double beta decay search, *Nucl. Instr. Meth. A* **729**, 856 (2013).
- [285] L. Berge et al., Purification of molybdenum, growth and characterization of medium volume  $\text{ZnMoO}_4$  crystals for the LUMINEU program, *JINST* **9**, P06004 (2014).
- [286] E. Armengaud et al., Development and underground test of radiopure  $\text{ZnMoO}_4$  scintillating bolometers for the LUMINEU  $0\nu 2\beta$  project, *JINST* **10**, P05007 (2015).
- [287] D.M. Chernyak et al., Effect of tungsten doping on  $\text{ZnMoO}_4$  scintillating bolometer performance, *Opt. Mat.* **49**, 67 (2015).
- [288] V. Grigorieva et al.,  $\text{Li}_2\text{MoO}_4$  Crystals Grown by Low-Thermal-Gradient Czochralski Technique, *J. Mat. Sci. Engineering B* **7**, 63 (2017).
- [289] F.A. Danevich, R&D of radiopure crystal scintillators for low counting experiments, presented at the Workshop on Radiopure scintillators for EURECA (RPSCINT 2008), 9-10 September 2008, Kyiv, Ukraine, p. 72, arXiv:0903.1539 [nucl-ex].
- [290] R. Bernabey et al., Production of high-pure Cd and  $^{106}\text{Cd}$  for  $\text{CdWO}_4$  and  $^{106}\text{CdWO}_4$  scintillators, *Metallofizika i Noveishie Tekhnologii* **30** (spec. issue), 477 (2008) (in Russian).
- [291] G.P. Kovtun et al., Production of radiopure natural and isotopically enriched cadmium and zinc for low background scintillators, *Functional Materials* **18**, 121 (2011).

- [292] R.S. Boiko et al., Ultrapurification of archaeological lead, *Inorg. Mater.* **47**, 645 (2011).
- [293] V.N. Shlegel et al., Recent progress in oxide scintillation crystals development by low-thermal gradient Czochralski technique for particle physics experiments, *JINST* **12**, C08011 (2017).
- [294] F.A. Danevich, Development of Crystal Scintillators From Enriched Isotopes for Double  $\beta$  Decay Experiments, *IEEE Trans. Nucl. Sci.* **59**, 2207 (2012).